NAVAL POSTGRADUATE SCHOOL

MONTEREY, CALIFORNIA

THESIS

ADDITIVE MANUFACTURING OF CERAMIC COMPOSITES FOR THERMAL PROTECTION SYSTEMS

by

Kelly M. Raisch

June 2020

Thesis Advisor: Ibrahim E. Gunduz
Co-Advisor: Claudia C. Luhrs

THIS PAGE INTENTIONALLY LEFT BLANK

REPORT DOCUMENTATION PAGE	*Form Approved OMB No. 0704-0188*

1. AGENCY USE ONLY *(Leave blank)*	**2. REPORT DATE** June 2020	**3. REPORT TYPE AND DATES COVERED** Master's thesis

4. TITLE AND SUBTITLE
ADDITIVE MANUFACTURING OF CERAMIC COMPOSITES FOR THERMAL PROTECTION SYSTEMS

5. FUNDING NUMBERS

6. AUTHOR(S) Kelly M. Raisch

7. PERFORMING ORGANIZATION NAME(S) AND ADDRESS(ES)
Naval Postgraduate School
Monterey, CA 93943-5000

8. PERFORMING ORGANIZATION REPORT NUMBER

9. SPONSORING / MONITORING AGENCY NAME(S) AND ADDRESS(ES)
N/A

10. SPONSORING / MONITORING AGENCY REPORT NUMBER

11. SUPPLEMENTARY NOTES The views expressed in this thesis are those of the author and do not reflect the official policy or position of the Department of Defense or the U.S. Government.

12a. DISTRIBUTION / AVAILABILITY STATEMENT
Approved for public release. Distribution is unlimited.

12b. DISTRIBUTION CODE
A

13. ABSTRACT (maximum 200 words)

The study and use of the space domain, including the recent reinvigoration of manned space exploration to the moon and beyond, drives the search for higher-performance materials for spacecraft thermal protection systems (TPSs). Ceramics and high-performance carbon both exhibit material properties that are suitable for TPS applications, but their performance can be maximized using additive manufacturing (AM) methods. Vibration-assisted printing (VAP) is a newly developed AM process that can fabricate parts using highly viscous mixtures of ceramic-forming polymers with solid ceramic particles. This work explores the AM of a ceramic sandwich TPS utilizing VAP. The TPS outer layers consist of silicon carbide (SiC) for high oxidation resistance, high melting point, and low thermal conductivity. A thin middle layer consists of a carbon-based material that provides high in-plane thermal conductivity to redistribute heat. Numerical simulations showed that this configuration was effective at reducing maximum temperatures under simulated re-entry conditions. A highly viscous mixture was prepared from a polycarbosilane polymer and pure SiC powder, which could be 3D-printed using VAP, and the middle layers for assembly were printed via standard thermoplastic extrusion using carbon-loaded or carbon-fiber-loaded filaments. SiC components were cured up to 248.8°C and pyrolyzed at up to 1,600°C, and were characterized via SEM, EDS, and XRD and tested for compressive strength.

14. SUBJECT TERMS
thermal protection system, TPS, additive manufacturing, AM, vibration-assisted printing, VAP

15. NUMBER OF PAGES
107

16. PRICE CODE

17. SECURITY CLASSIFICATION OF REPORT	**18. SECURITY CLASSIFICATION OF THIS PAGE**	**19. SECURITY CLASSIFICATION OF ABSTRACT**	**20. LIMITATION OF ABSTRACT**
Unclassified	Unclassified	Unclassified	UU

NSN 7540-01-280-5500

Standard Form 298 (Rev. 2-89)
Prescribed by ANSI Std. 239-18

THIS PAGE INTENTIONALLY LEFT BLANK

Approved for public release. Distribution is unlimited.

ADDITIVE MANUFACTURING OF CERAMIC COMPOSITES FOR THERMAL PROTECTION SYSTEMS

Kelly M. Raisch
Major, United States Marine Corps
BS, California Polytechnic State University, 2006

Submitted in partial fulfillment of the
requirements for the degree of

MASTER OF SCIENCE IN SPACE SYSTEMS OPERATIONS

from the

NAVAL POSTGRADUATE SCHOOL
June 2020

Approved by: Ibrahim E. Gunduz
Advisor

Claudia C. Luhrs
Co-Advisor

James H. Newman
Chair, Space Systems Academic Group

THIS PAGE INTENTIONALLY LEFT BLANK

ABSTRACT

The study and use of the space domain, including the recent reinvigoration of manned space exploration to the moon and beyond, drives the search for higher-performance materials for spacecraft thermal protection systems (TPSs). Ceramics and high-performance carbon both exhibit material properties that are suitable for TPS applications, but their performance can be maximized using additive manufacturing (AM) methods. Vibration-assisted printing (VAP) is a newly developed AM process that can fabricate parts using highly viscous mixtures of ceramic-forming polymers with solid ceramic particles. This work explores the AM of a ceramic sandwich TPS utilizing VAP. The TPS outer layers consist of silicon carbide (SiC) for high oxidation resistance, high melting point, and low thermal conductivity. A thin middle layer consists of a carbon-based material that provides high in-plane thermal conductivity to redistribute heat. Numerical simulations showed that this configuration was effective at reducing maximum temperatures under simulated re-entry conditions. A highly viscous mixture was prepared from a polycarbosilane polymer and pure SiC powder, which could be 3D-printed using VAP, and the middle layers for assembly were printed via standard thermoplastic extrusion using carbon-loaded or carbon-fiber-loaded filaments. SiC components were cured up to 248.8°C and pyrolyzed at up to 1,600°C, and were characterized via SEM, EDS, and XRD and tested for compressive strength.

THIS PAGE INTENTIONALLY LEFT BLANK

TABLE OF CONTENTS

LIST OF FIGURES

THIS PAGE INTENTIONALLY LEFT BLANK

LIST OF TABLES

THIS PAGE INTENTIONALLY LEFT BLANK

LIST OF ACRONYMS AND ABBREVIATIONS

AM	Additive Manufacturing
CMC	Ceramic-Matrix Composites
CVI	Chemical Vapor Infiltration
DSC	Differential Scanning Calorimetry
EDS	Energy-Dispersive X-ray Spectroscopy
FDM	Fused Deposition Modeling
FLIR	Forward-Looking Infrared
IR	Infrared
JCPDF	Joint Committee of Powder Diffraction Files
LOM	Laminated Object Manufacturing
ME	Material Extrusion
MPCV	Multi-purpose Crew Vehicle
NASA	National Aeronautics and Space Administration
PCP	Pre-Ceramic Polymers
PCS	Polycarbosilane
PDC	Polymer-Derived Ceramics
PICA	Phenolic Impregnated Carbon Ablator
PIP	Polymer Infiltration and Pyrolysis
PLA	Polylactic Acid
PVA	Polyvinyl Alcohol
RCC	Reinforced Carbon-Carbon
RPM	Revolutions Per Minute
SEM	Scanning Electron Microscopy
SiC	Silicon Carbide
Si_3N_4	Silicon Nitride
SLS	Selective Laser Sintering
TGA	Thermogravimetric Analysis
TPS	Thermal Protection System
VAO	Vacuum Oven
VAP	Vibration-Assisted Printing

VP	Vat Photopolymerization
XRD	X-ray Diffraction

ACKNOWLEDGMENTS

I would like to thank my thesis advisors, Doctors Emre Gunduz and Claudia Luhrs. Without their guidance, knowledge, support, and patience, this research would not have been possible. Doctor Gunduz's consistent hands-on assistance in laboratory research was crucial to the success of this work and facilitated the preponderance of my education in additive manufacturing and material science. I am truly grateful for the devoted time and patience, which was needed to have made such progress. I would also like to thank Doctor Troy Ansell for his training and assistance with various laboratory equipment used in material characterization.

I would also like to express my gratitude to the Space Systems Academic Group. I would like to thank Doctor James Newman for his wisdom in choosing a research topic. I would like to thank Doctor Wenschel Lan and Dan Sakoda for their assistance in modeling and simulation and spacecraft engineering considerations. I would also like to thank Lieutenant Kenneth Wooten for assistance with material preparation and sample characterization during periods of overlap in our respective thesis work. "Sharing the workload" during these periods certainly enabled greater progress for us both.

Finally, I would like to thank my family—most especially my wife, Jessica—for their unwavering support and patience during the countless hours spent conducting this research. Their love and support have kept me grounded throughout my career in the Marine Corps and were absolutely pivotal to the success I've enjoyed here as a graduate student.

THIS PAGE INTENTIONALLY LEFT BLANK

I. INTRODUCTION

A. MOTIVATION

The space domain continues to be an area of great interest and benefit for scientific, commercial, and military applications. Satellites provide invaluable capabilities such as imagery, weather and environmental monitoring, and communications, to name a few. Likewise, manned spaceflight has taken mankind to the moon and provides a means of scientific research not otherwise possible on Earth. While many satellites and probes are launched into space with no expectation of an intact return, such returns are considered "no fail" missions for all manned spaceflights. This makes manned spaceflight a very complex and difficult feat, yet the concept has been reinvigorated in a United States Presidential Policy Directive to "lead an innovative and sustainable program of exploration … across the solar system and to bring back to Earth new knowledge and opportunities" [1]. A key component for a safe return of any spacecraft is the spacecraft's thermal protection system (TPS), often referred to as heat shielding. With a rich history in manned spaceflight, the United States has explored and utilized several concepts and materials for spacecraft TPS, most notably those used in the Apollo and Space Shuttle programs.

All TPS materials can be categorized as either ablative or non-ablative. Ablative materials used in TPS offer protection of the re-entry vehicle through the sacrificial erosion of the material under very high temperature and pressure. This results in "the removal of material by a combination of thermo-mechanical, thermo-chemical, and thermo-physical factors with high temperature, pressure, and velocity of combustion flame" [2]. A well-known example of an ablative TPS is the Avcoat material developed and used on the Apollo Command Modules in the 1960s and 1970s (Figure 1) [3]. The material was highly effective, but was also a single-use material with a convoluted and costly manufacturing process [3]. Greater cost-effectiveness could be achieved through the development and implementation of a non-ablative, reusable TPS material, which is especially relevant for the current proliferation of commercial launches.

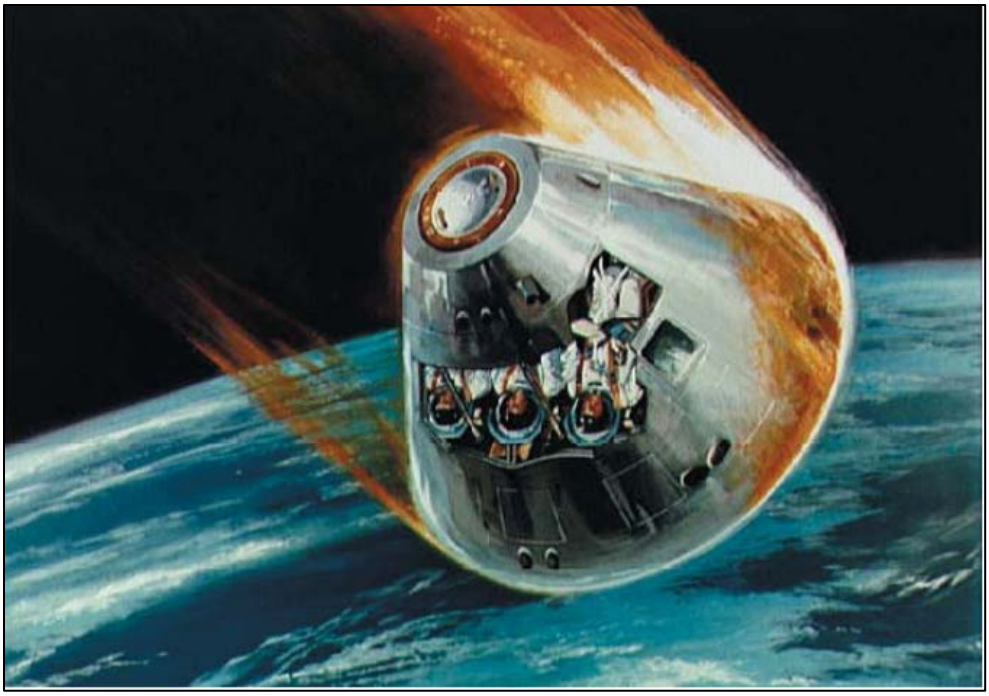

Figure 1. Artistic Rendition of Apollo Capsule Re-entry. Source: [4].

While non-ablative materials make for more cost-effective space operations, these materials must be just as effective and reliable as ablative materials and have the ability to withstand the extremely violent conditions of high-velocity re-entry without deformation or degradation to their mechanical and thermal protective properties. A well-known example of a non-ablative TPS is the highly porous silica (SiO_2)-based tiles utilized on the Space Shuttle [3]. These tiles proved to be lightweight and effective at withstanding the extreme thermal conditions, but were also fragile and exhibited several points of damage after every Space Shuttle mission [5]. Likewise, the reinforced carbon-carbon (RCC) material used for the Space Shuttle wing's leading edge was significantly stronger than the silica tiles, but still prone to damage during shuttle missions [6].

The ideal TPS is a re-usable, non-ablative material that is strong, lightweight, relatively easy and inexpensive to manufacture, simple to replace when needed, and able to withstand the extreme environments of space and atmospheric re-entry. This research explores specific methods of additive manufacturing to produce layered composites that have been designed to exhibit suitable thermal and structural properties. The completed

material should be strong, lightweight, and exhibit low thermal conductivity in the direction normal to the material's surface. The material should also exhibit higher in-plane thermal conductivity in order to redistribute heat to the rest of the structure, thus lowering the maximum temperatures encountered and improving TPS performance and overall lifespan.

B. BACKGROUND

1. History of TPS Materials

The United States has a rich history of space exploration dating back to the early 1960s. During this time period, human spaceflight missions continued to increase in complexity and audacity, with the ultimate capstone of sending Americans to the moon and safely returning them to Earth. A very important component for the success of this mission was a reliable TPS that was able to withstand the extreme pressure and temperature of re-entry through the Earth's atmosphere. Project Mercury and the Gemini Program required heatshields (TPS) to withstand Earth-orbit re-entries with a velocity of approximately 7.9 km/s; however, the Apollo Program required its capsule to withstand a lunar-return trajectory resulting in a re-entry velocity of approximately 11 km/s, thus resulting in an aerodynamic heating environment approximately four times as severe as the Mercury and Gemini capsules [7].

The ablator adopted for the Apollo capsule TPS was developed by the Avco Corporation, officially designated Avco 5026–39G [7], also referred to as Avcoat [3]. Avcoat is an epoxy-novalac resin reinforced with quartz fibers and phenolic microballoons and has a density of 31 lb/ft^3 (496 kg/m^3) [7]. It formed the outer region of a multilayered TPS that also consisted of insulating materials as well as aluminum and stainless-steel honeycomb substructures, with thicknesses that varied with location on the spacecraft (Figure 2) [7].

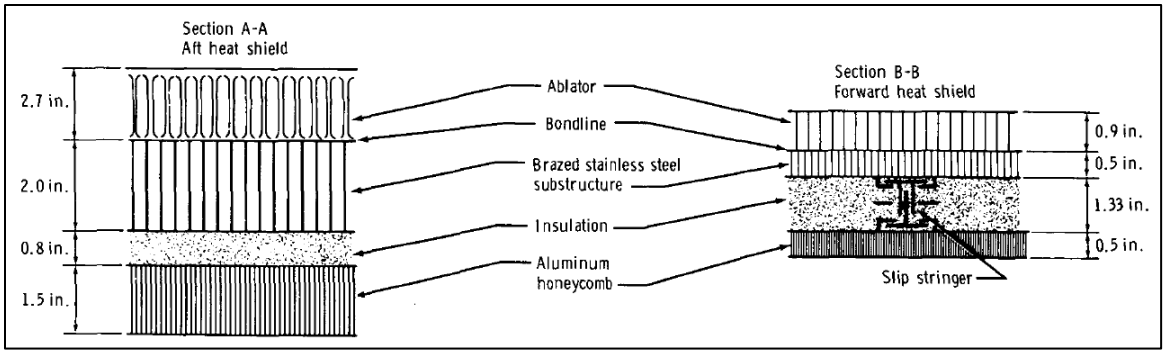

Figure 2. Structural Arrangement of Apollo TPS. Source: [7].

Furthermore, the surface of the Avcoat was covered with pressure-sensitive Kapton polyimide tape coated with aluminum and oxidized silicon monoxide, in order to ensure an absorptance-to-emittance ratio of 0.4 for proper thermal control of the spacecraft throughout its mission [7].

The fabrication of the Apollo TPS consisted of several steps. Brazed sandwich panels of stainless-steel were welded together before being sent to Avco Corporation for application of the ablator [7]. Once at Avco, the structure was cleaned with an abrasive detergent slurry and then coated with a primer [7]. A fiberglass honeycomb was then bonded to the structure with tape adhesive [7]. The Avcoat material was applied by "gunning" (injecting) the ablator into the honeycomb cells (Figure 3) and subsequently cured for 16 hours and post-cured for 16 hours at 200°F and 250°F, respectively [7].

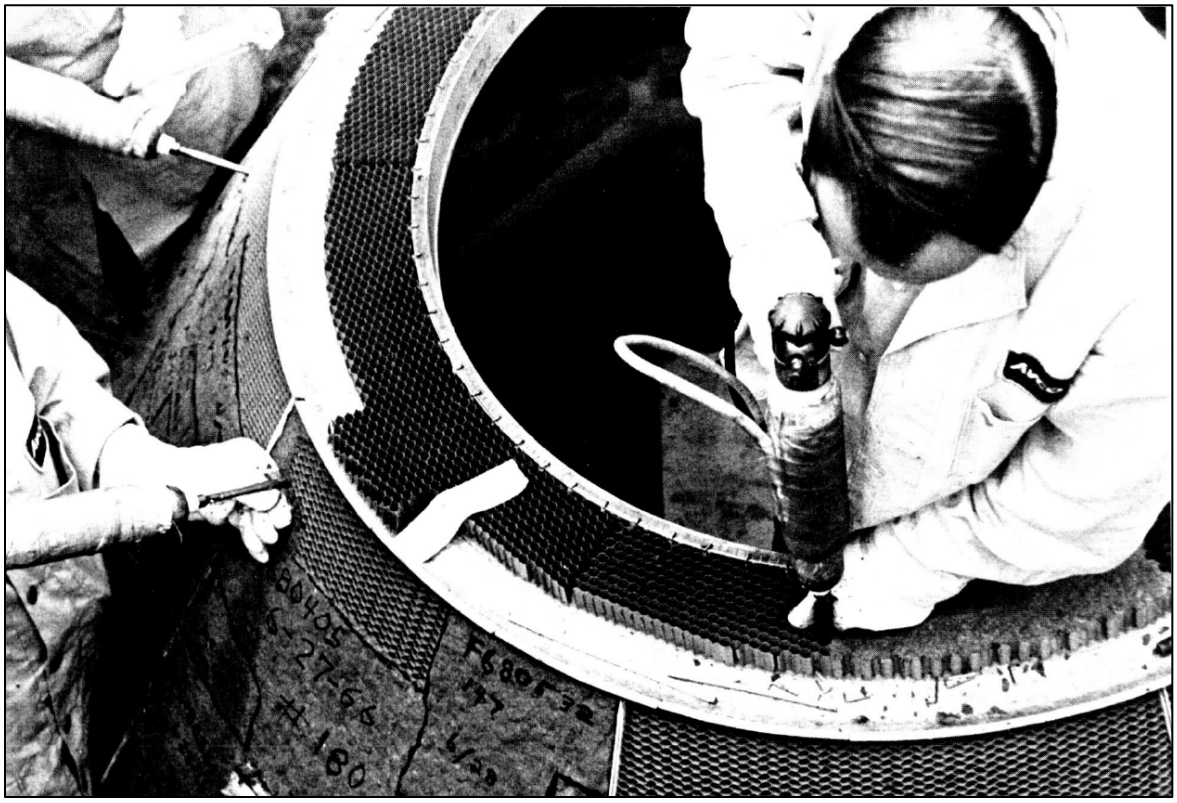

Figure 3. ”Gunning” of Avcoat into Honeycomb Cells. Source: [7].

Finally, the surface was machined with a lathe to the required design thickness before it was sealed with a thin layer of epoxy-based pore sealer and a moisture-protective plastic coating [7].

The National Aeronautics and Space Administration (NASA) explored the potential usage of Avcoat as a TPS material for a more recent mission: the Multi-purpose Crew Vehicle (MPCV), also known as the Orion capsule [3]. Approximately $25 million and five years were invested in recreating Avcoat, which proved to be a complex process requiring hand-assembly spanning nine steps (Figure 4) [3].

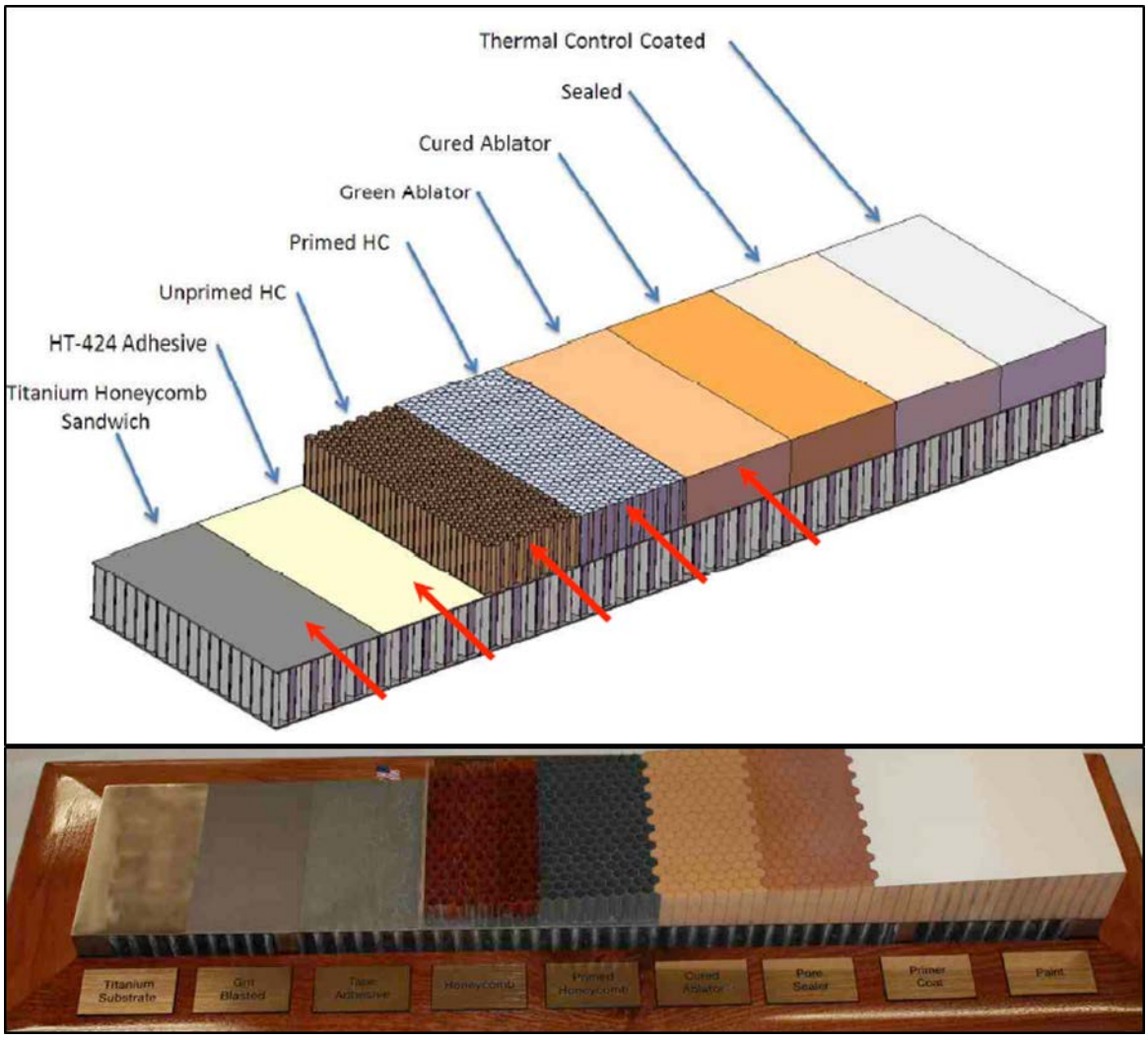

Figure 4. Avcoat Process Steps for MPCV. Source: [3].

In the end, Phenolic-Impregnated Carbon Ablator (PICA) was the favored TPS material for the mission. PICA is a much more recently developed and proven [8] TPS ablator with a very low density (~270 kg/m^3) compared to Avcoat [3].

The space shuttle program utilized reusable, non-ablative materials for its TPS. The majority of each space shuttle orbiter was covered with 24,300 silica-based tiles (Figure 5), which were designed to survive up to 100 missions [9]. All tiles (LI-900) are made up of a glass composite of silica, alumina fiber, and borosilicate that are formed by molding and compressing an aqueous solution, then microwaving and heat treating at 1,288 °C [9]. The tiles on the top and sides of the orbiter were white coated Low-temperature Reusable

Surface Insulation which could withstand up to 650 °C [9]. The tiles on the bottom and front of the orbiter were black coated High-temperature Reusable Surface Insulation tile which could withstand up to 1,260 °C [9]. The LI-900 material in the tiles exhibit an incredibly low density of 144.2 kg/m^3, due to the extreme porosity of the material [10].

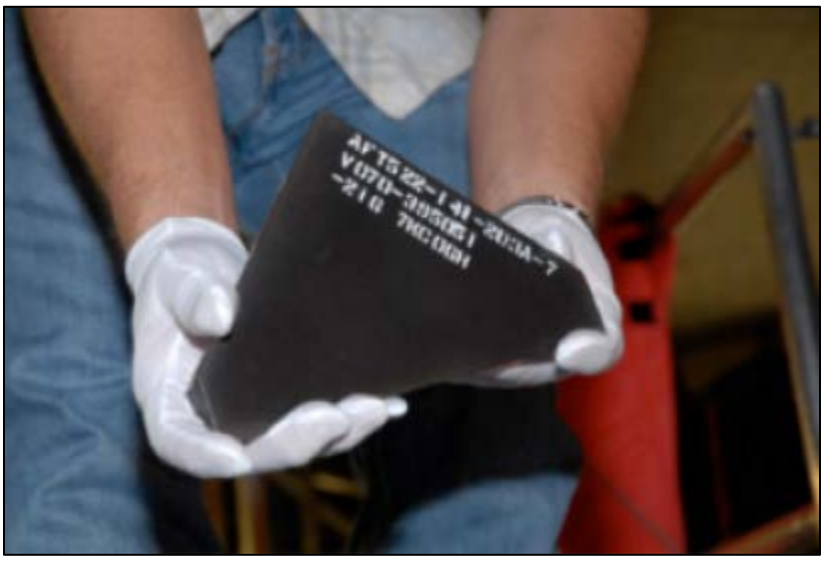

Figure 5. Space Shuttle Orbiter Tile. Source: [9]

While the silica tiles could withstand the extreme temperatures, a material with stronger mechanical properties was needed for the leading edges and nose cone of the space shuttle orbiter. This was accomplished with the development and implementation of RCC, developed by Ling-Temco-Vought [6]. The fabrication of RCC is summed up in chapter 3 of the Columbia Accident Investigation Board report:

> The basic RCC composite is a laminate of graphite-impregnated rayon fabric, further impregnated with phenolic resin and layered, one ply at a time, in a unique mold for each part, then cured, rough-trimmed, drilled, and inspected. The part is then packed in calcined coke and fired in a furnace to convert it to carbon and is made more dense by three cycles of furfuryl alcohol vacuum impregnation and firing.
>
> To prevent oxidation, the outer layers of the carbon substrate are converted into a 0.02-to-0.04-inch-thick layer of silicon carbide in a chamber filled with argon at temperatures up to 3,000 degrees Fahrenheit. As the silicon carbide cools, “craze cracks” form because the thermal expansion rates of

the silicon carbide and the carbon substrate differ. The part is then repeatedly vacuum-impregnated with tetraethyl orthosilicate to fill the pores in the substrate, and the craze cracks are filled with a sealant. [6]

Research continues in the search for better reusable TPS materials and manufacturing processes. While the Space Shuttle Orbiter TPS was effective at protecting the spacecraft throughout each mission, it was estimated to incur 40,000 hours of maintenance between flights [11]. During the development of the X-33 program, NASA began research into a metallic TPS (Figure 6), with detailed design and fabrication conducted by BF Goodrich, Aerostructures Group [11]. This new TPS incorporated titanium multiwall and superalloy honeycomb structures lined with lightweight fibrous insulation [11].

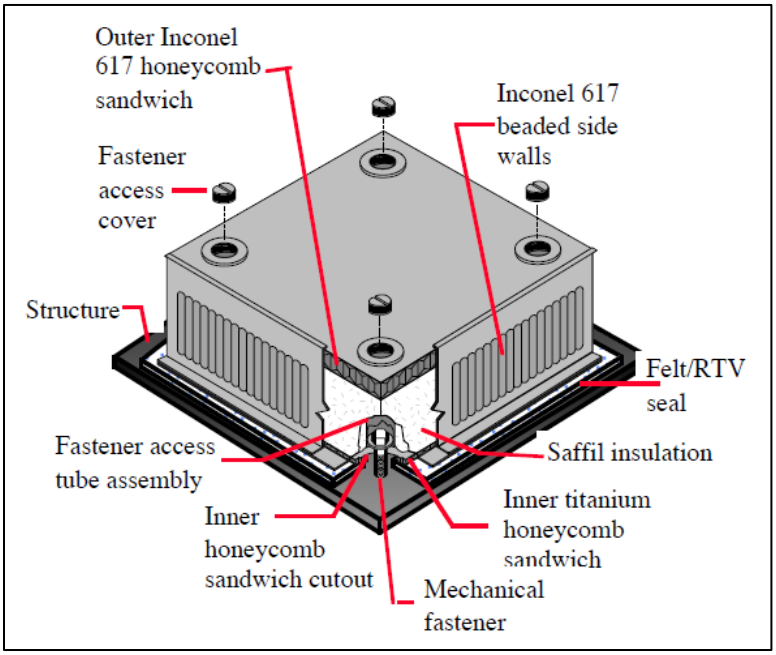

Figure 6. Superalloy Honeycomb Sandwich TPS. Source: [11].

The use of high-performance ceramics for improved TPS materials has been the subject of much research within the last three decades. C-SiC CMC structures were developed and tested during research in the 1990s for both TPS [12] and braking applications [13]. More recent research has proposed the development of CMCs with

additional layers for a more efficient TPS: a sandwich structure with CMC outer layers and a SiC foam or lattice middle layer used to pass coolant for active cooling, as shown in Figure 7 [14]. Several "Smart TPS" concepts have also been proposed, including "self-healing" TPS materials where CMC microcracks are immediately sealed before oxygen reaches inner fibers [15]. AM of TPS materials has also been researched using FDM to fabricate TPS components with polyetherimide polymer [16].

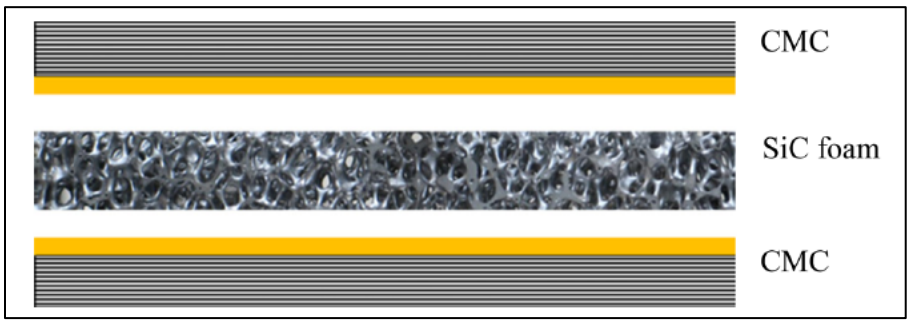

Figure 7. Ceramic Sandwich TPS Concept. Source: [14].

2. Additive Manufacturing

Additive Manufacturing (AM), also commonly referred to as "3D printing," can generally be described as the creation of objects by depositing constituent materials in layers using 3D models [17]. The process requires four basic components: (1) a digital model of the object to be created, (2) the materials to create the object, (3) a tool for distributing the material/s, and (4) a digital control system for the tool to distribute the material/s in accordance with the digital model [17]. This approach to manufacturing provides a plethora of benefits, including greater customization with complex internal features and hollow or lattice structures and material gradients, thus improving various performance parameters and manufacturing efficiency [17]. AM has been applied to a variety of materials, including plastics, metals, ceramics, and even food.

According to a report on the history of AM [18], the first true form of AM was a process developed in the 1980s called stereolithography; however, its roots stem from a much earlier point in time. In the late 1960s, an experiment was conducted at Battelle

Memorial Institute involving intersecting two laser beams of different wavelengths into a vat of photopolymer resin [18]. The aim of the experiment was to polymerize the resin at the point of intersection of the lasers [18]. Work continued for many years in an attempt to develop this method further, but never produced a commercially available system [18].

A similar dual-laser prototyping method was demonstrated in the early 1970s, which was called "photochemical machining," shown in Figure 8 [18]. In the late 1970s, a new method called "solid photography" was patented by Dynell Electronics Corp [18]. This new process produced a 3D object by cutting cross sections under computer control, with a milling machine or laser, and stacking them to form a specific shape [18]. This company later merged with United Technologies and continued to develop and commercialize this technology under different names through the 1980s [18].

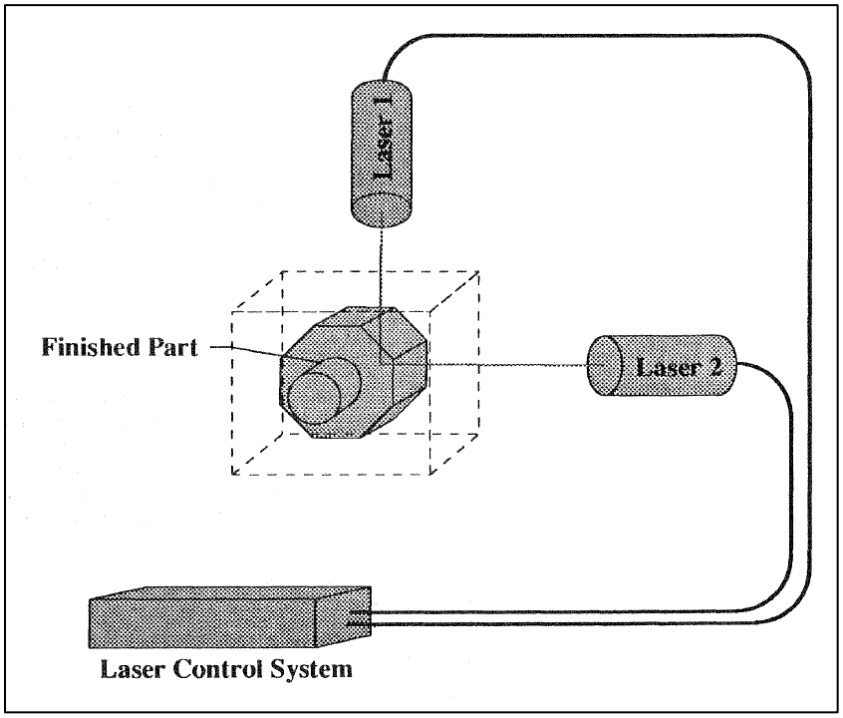

Figure 8. Photochemical Machining Apparatus. Source: [19].

Stereolithography, the "first working additive manufacturing technique," was originally envisioned by Hideo Kodama at the Nagoya Municipal Industrial Research

Institute in Nagoya, Japan [18]. He was among the first to invent the single-beam laser curing approach, and published multiple papers leading to the development of stereolithography [18]. He experimented with using black and white film to mask and control UV exposure on a photosensitive resin for each cross-section, as well as concentrating a spot of UV light through an optical fiber controlled by a plotter (Figure 9) [18]. Kodama further describes a key element of stereolithography: "If the solidified layer is immersed into the liquid with the top at a depth equal to the thickness of the layer to be solidified, its top surface is covered with unsolidified liquid polymer" [18]. Stereolithography, as well as other approaches to AM, continued to develop scientifically and commercially throughout the 1980s and 1990s with varying success [18].

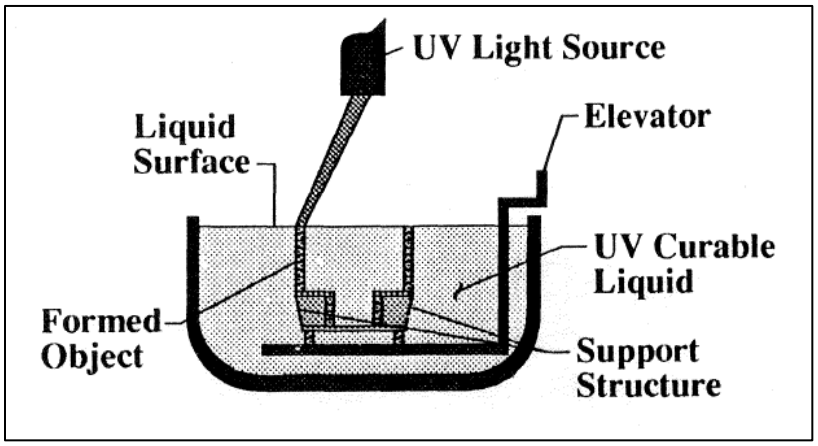

Figure 9. Stereolithography Apparatus. Source: [19].

Several new techniques of AM were developed and commercialized throughout the 1990s. Stratasys developed fused deposition modeling (FDM) whereby thermoplastic filaments are extruded in layers to produce three-dimensional objects [18]. Cubital developed solid ground curing which uses UV light through an electrostatic toner mask in glass to solidify a UV-sensitive liquid polymer [18]. Helisys developed laminated object manufacturing (LOM) which uses a digitally-guided laser to bond and cut sheet material (Figure 10) [18]. Selective laser sintering (SLS) was developed by DTM using powdered materials that are fused under heat from a laser (Figure 11) [18]. Direct shell production casting, commercialized by Soligen in 1993, used an inkjet mechanism to deposit liquid

binder onto ceramic powder to form shells [18]. Improvements in AM continued through the 1990s and early 2000s with smaller and less-expensive machines and more efficient and unique techniques, including laser additive manufacturing to fuse powdered titanium alloys, as well as controlled metal buildup and direct metal deposition [18].

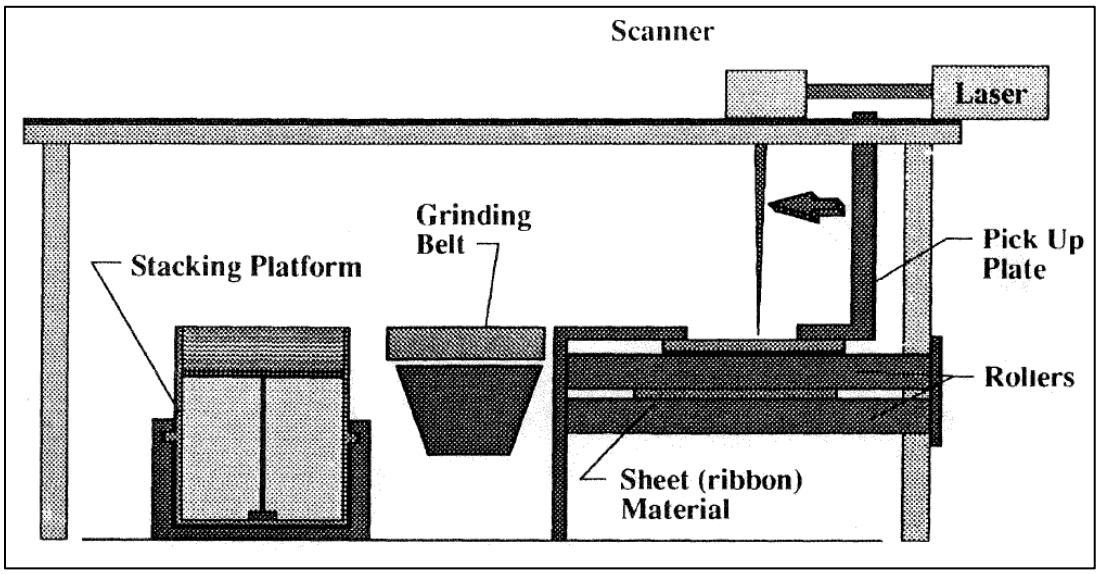

Figure 10. Laminated Object Manufacturing (LOM). Source: [19].

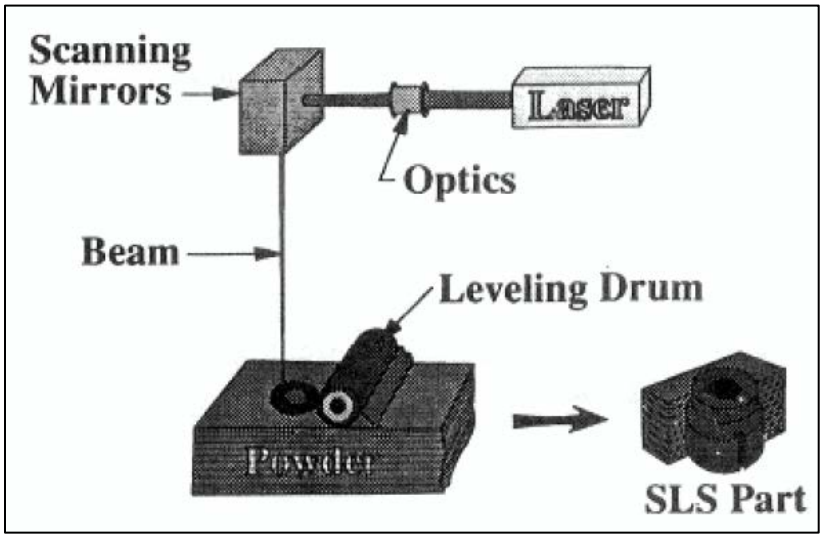

Figure 11. Selective Laser Sintering (SLS). Source: [19].

According to the International Organization for Standardization and American Society for Testing and Materials, AM processes are currently classified into the following seven categories: (1) binder jetting, (2) directed energy deposition, (3) material extrusion (ME), (4) material jetting, (5) powder bed fusion, (6) sheet lamination, and (7) vat photopolymerization (VP) [17]. A much more recently developed form of ME is vibration-assisted printing (VAP), which ultimately allows for the AM of highly viscous materials [20].

VAP vastly increases the range of materials available for AM due to its ability to extrude highly viscous materials. This technique uses high-amplitude ultrasonic vibrations to induce the controlled flow of a highly viscous material under pressure [20]. First, a reservoir such as a plastic syringe with a 0.6 mm nozzle tip is filled with a viscous, clay-like material and pressurized, typically in the range of 35–850 kPa depending on the material's viscosity [20]. With only pressure applied, the material does not flow through the syringe tip due to the flow resistance from the fine nozzle opening; however, when the tip of the nozzle is vibrated at an ultrasonic resonant frequency, the material will begin to extrude freely through the nozzle tip [20]. The flow rate can then be controlled by adjusting the amount of pressure and the amplitude of the vibration [20]. When integrated into a 3D printing machine (see Figure 12 for conceptual setup), objects can be created using more viscous materials [20]. The ability to extrude and print highly viscous materials enables the AM of high solids loaded mixtures of solid particles with binders, demonstrated at 76 vol.% and possibly higher, much higher than any other AM process [21]. The particles in such mixtures are in contact, so the mixtures exhibit yield strength and plasticity, which is advantageous to AM [21]. Furthermore, post-processing processes like sintering results in less shrinkage due to the high solids content.

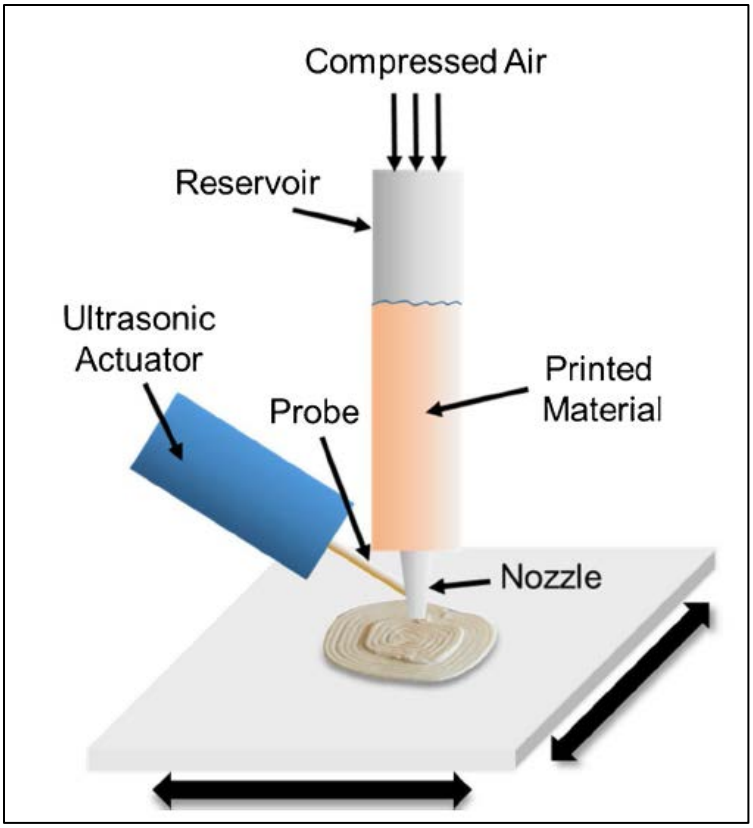

Figure 12. Conceptual VAP Setup. Source: [20].

3. Ceramic-Matrix Composites

Ceramics have been studied and used for various high-performance applications commercially and industrially, to include aerospace and hypersonics [22], engine and braking systems [23], and much more. Many of these high-performance ceramics are silicon-based with varying properties and methods of formation and manipulation for manufacturing of parts. Since such ceramics are designed with the ability to withstand extremely high temperatures, such as exceeding 2000°C during hypersonic flight [24], manipulation of the ceramic once it is formed can prove difficult. One very effective means of producing ceramic parts is through the use of polymer-derived ceramics (PDCs) [23]. PDCs, including ceramic-matrix composites (CMCs), can be formed through various methods, such as melt-infiltration (MI), chemical-vapor infiltration (CVI), and polymer infiltration and pyrolysis (PIP) [24]. The usage of pre-ceramic polymers (PCPs) in the manufacturing of CMCs is widely used over CVI or MI with advantages in cost-reduction,

lower process temperatures, as well as the ability to produce large, complex parts [23]. Silicon-based PCPs, very common for use in CMCs, are shown in Figure 13.

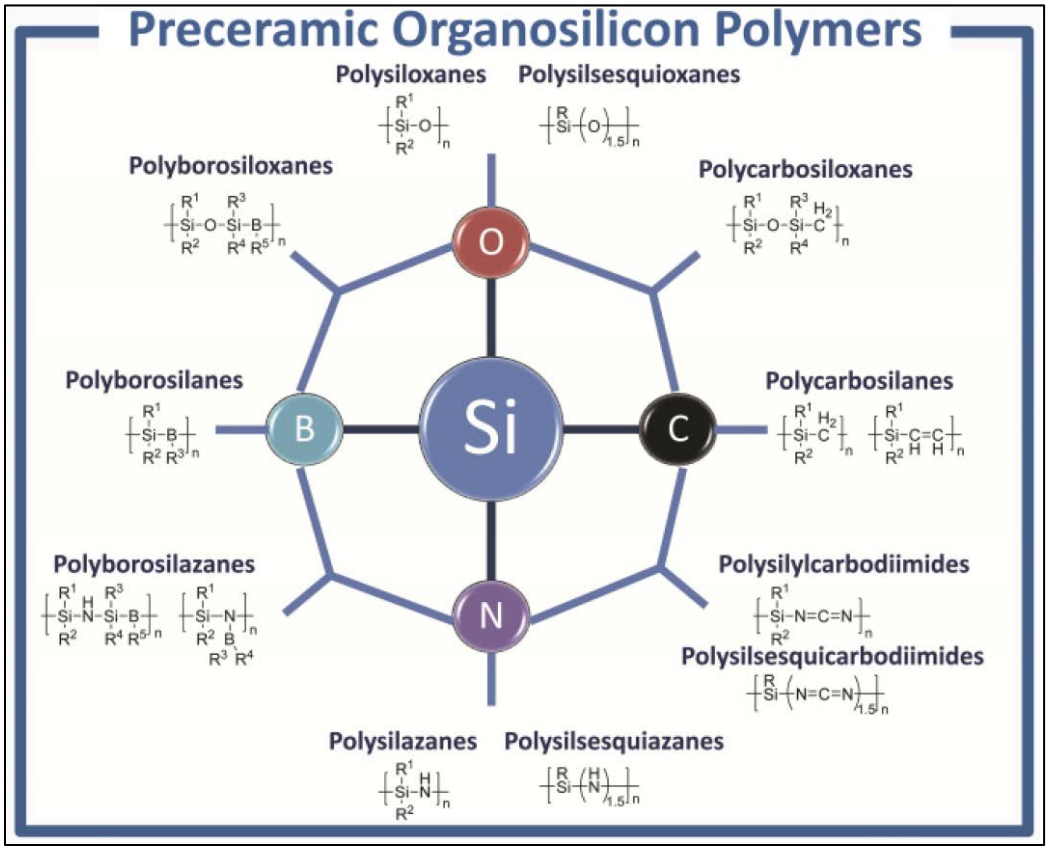

Figure 13. Silicon-Based PCPs. Source: [23].

Silicon carbide (SiC) ceramics have been proven to exhibit many high-performance characteristics, including resistance to high temperature, oxidation, corrosion, and thermal shock [25]. Fabrication of monolithic SiC materials can be achieved within a variety of methods, such as powder sintering, sol-gel, chemical vapor deposition, and polymer conversion [25]. Formation of SiC through a polycarbosilane (PCS) precursor provides advantages in facilitating the manufacturing of SiC parts in complex shapes at relatively moderate temperatures [25]. Ideal PCS resins should have a low cure temperature, high ceramic yield, near-stoichiometric elemental ratio, excellent thermal stability, and viscosity that promotes easy material processing [25].

The formation of SiC ceramics from PCPs follows a process common to most PDCs, as shown in Figure 14. The polymer is first synthesized from monomer or oligomer precursors, which can be adjusted through pre-curing [26]. The polymer is then formed into the desired object shape before thermal-induced curing at 150°C-250°C [26]. Finally, the cured polymer is crystallized through pyrolysis at 500°C-1,600°C to create a ceramic with a desired shape [26]. However, these ceramic parts are highly porous after pyrolysis due to the removal of organic groups and elements (H, N, O, etc.) from the polymers, requiring methods like PIP, applied repeatedly to sequentially fill the voids. Ceramic powders can also be introduced into the polymer prior to curing to optimize the viscosity during manufacturing of CMCs and reduce shrinkage [24], which has been recently used for AM using VP [27] to a limited extent and VAP to produce silicon oxycarbide-short carbon fiber [28].

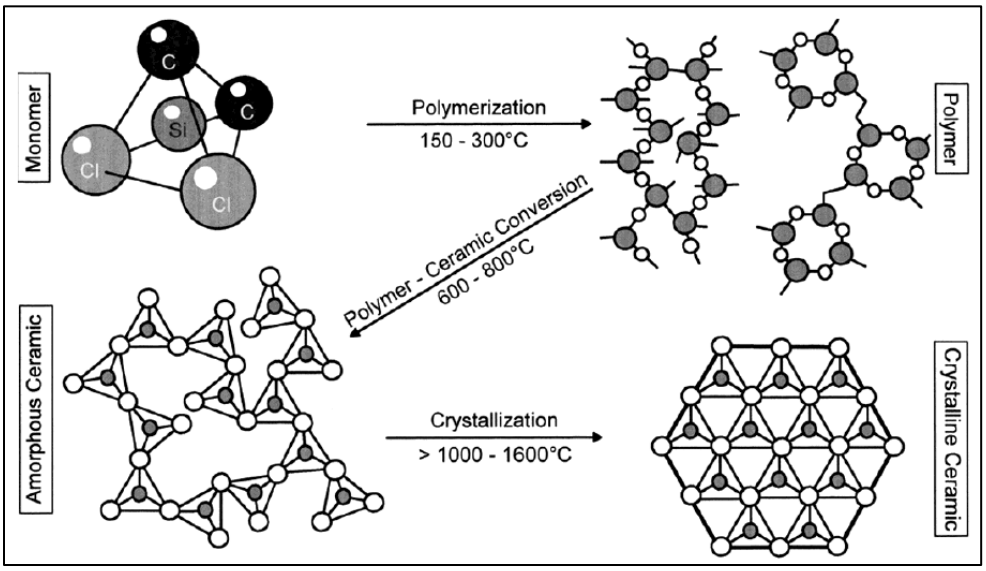

Figure 14. Ceramic Formation from Polymer Precursors. Source: [26].

C. OBJECTIVES

This project investigates the AM of SiC CMCs utilizing VAP. Beginning with a commercially available polycarbosilane PCP (StarPCS SMP-10 from Starfire Systems), high concentrations of SiC ceramic powders will be mixed into the polymer to create a highly viscous, clay-like material for VAP. PCP preparation will include an elevated temperature hold under vacuum prior to powder loading in order to induce higher mass loss prior to printing with the material, in an effort to reduce overall mass loss and associated shrinkage of the printed part during final curing and pyrolysis. Variations in heat treatment and powder loading will be explored in order to optimize a mixture ideally suited for VAP. Printed samples should exhibit a level of microporosity that reduces the mass and thermal conductivity of the printed part with little degradation in mechanical properties. For comparison, samples will be molded with the same material used for printing and analyzed using the same techniques used for the printed samples.

Once optimized for VAP, the powder-loaded PCP mixture will be used to create a sandwich sample similar to the concept shown in Figure 7. The outer layers will consist of SiC CMC and the middle layer will consist of a thinner layer of carbon (e.g., graphite), as shown in Figure 15. All layers will be 3D printed using a custom dual-head printer with both a FDM head and a VAP head. The boundaries of the structures and the inner carbonized layers will be printed with a thermoplastic filament such as polylactic acid (PLA), whereas the SiC parts will be printed using VAP of the optimized powder-loaded mixture to ultimately produce the ceramic structure, post-pyrolysis. The SiC CMC layers should provide strong, durable protection thermally and mechanically. The inner carbon layer should provide a passive means of thermal control, whereby heat is redistributed away from areas with the highest heat load, thus providing a more even distribution of heat across the TPS. To evaluate the validity of this idea, the thermal response of the proposed geometry will be modeled using a finite element package.

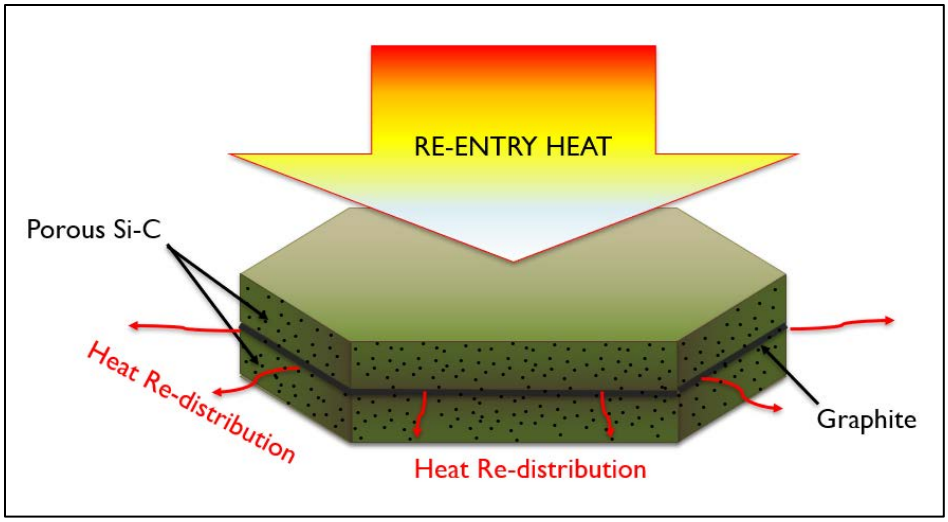

Figure 15. SiC CMC Sandwich TPS Concept

The results of this research should provide a basis for further research in both AM and TPS development through the following research questions and objectives:

- What is a suitable mixture formulation that enables AM of low porosity net-shaped parts?
- Will structures produced via VAP have improved characteristics compared to similar molded structures?
- Can 3D printing optimize fabrication of differing material layers for efficient heat redistribution to lower local temperatures?
- Can thermal conductivity be reduced with 3D printing engineered porosity without significantly compromising mechanical strength?

II. EXPERIMENTAL METHODS

A. MODELING AND SIMULATION

TPS sandwich layers were modeled using NX 12.0 by Siemens. The sandwich TPS concept was simulated by first modeling a section shaped as the leading-edge of a wing (Figure 16) with SiC layer thicknesses of 20 mm and a graphite layer thickness of 5 mm. 3D tetrahedral meshing (TET4) with 10 mm element size was applied to the SiC layers, with referenced material properties [29], [30]. Meshing can be seen in Figure 16 (right) on the outer face. 3D tetrahedral meshing (TET4) with 6 mm element size was applied to the graphite layer, with referenced material properties [31]. Referenced material data applied for SiC and graphite are shown in Table 1. An atmospheric re-entry heat load of 22.3 kW was applied to the front of the model (displayed as small red arrows in Figure 16 [right]), based on an estimated heat flux of 100 W/cm^2 [4]. An initial condition of 25°C was applied to the side and inside faces, displayed in blue in Figure 16 (right). Additionally, "perfect touching" boundary conditions were applied between layers. Transient thermal analysis was generated for durations of 60, 120, and 300 seconds (s) with a time step of 6 s. These are comparable to a re-entry condition (~300 s). The same simulation was repeated with the middle layer material properties converted to SiC for comparative analysis with a solid SiC leading edge to evaluate the effect of the graphite layer at the center.

Table 1. Material Properties Used for NX Simulation

Silicon Carbide	
Density (g/cm^3)	3.2
Thermal Expansion Coefficient (1/K)	8 x 10^{-6}
Thermal Conductivity (W/(m*K))	20
Specific Heat (J/(kg*K))	570
Graphite	
Density (g/cm^3)	1.6
Thermal Expansion Coefficient (1/K)	4 x 10^{-6}
Thermal Conductivity (W/(m*K))	200
Specific Heat (J/(kg*K))	770

SiC material properties sources: [29] and [30].

Graphite material properties source: [31].

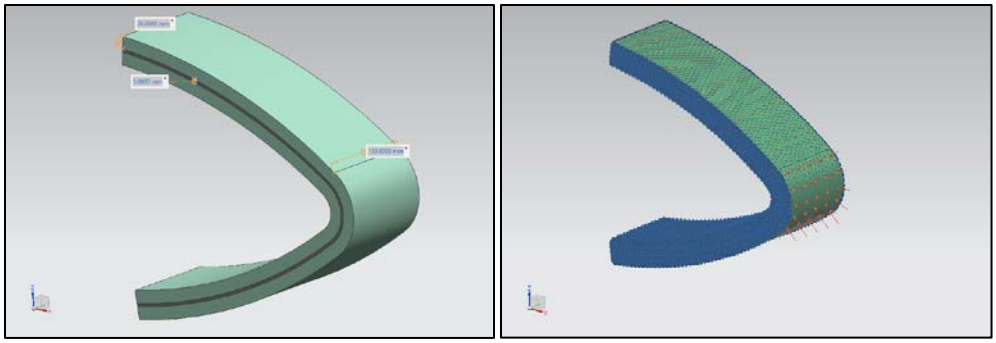

Figure 16. Wing Leading Edge TPS Model (left) and Simulation Conditions (right)

Tile samples for printing were modeled as 12.7 mm squares with 2.0 mm-thick SiC layers and 0.4 mm-thick graphite layer (Figure 17). The bottom SiC layer was modeled with a 0.4 mm "tray" in order to hold the printed graphite-forming layer. Models were exported as STL files, then processed for slicing to gcode files using Cura or Simplify 3D software.

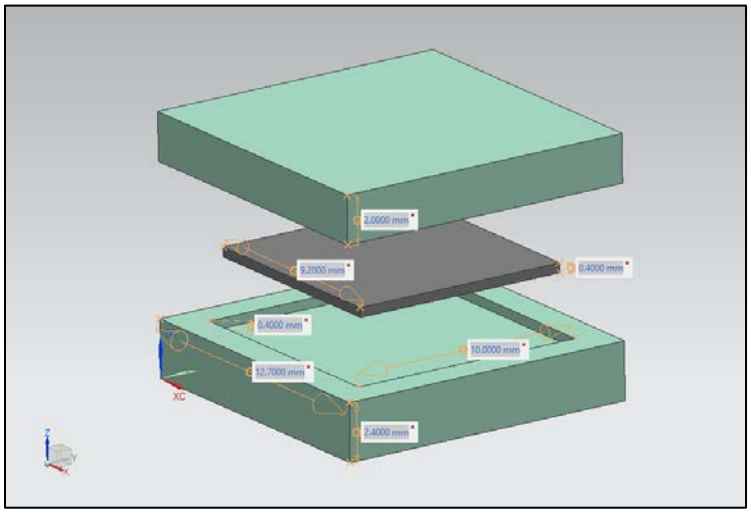

Figure 17. TPS Sandwich Tile Model

B. MATERIALS

Silicon carbide samples were created from a mixture of SiC powder and a polymer-forming binder. The SiC powder used was Sigma-Aldrich Co. -400 mesh particle size (Lot# MKBN2849V). The mesh size -400 refers to a mesh opening size of 38 μm. The polymer-forming binder used was StarPCS® SMP-10 from Starfire Systems, Inc (Lot# J-25086), which forms 1:1 stoichiometric ratio SiC when pyrolyzed [22]. The density of SMP-10 is 0.998 g/cm^3, according to the manufacturer [22]. Polylactic acid (PLA) filament was used to determine if a carbon-forming material interfaced with SiC would produce negative effects during curing or pyrolysis. In order to produce a carbon middle TPS layer upon pyrolysis, two filaments were used in separate samples to determine which produced better results: carbon-loaded PLA filament and carbon-fiber-loaded nylon filament.

C. SAMPLE PREPARATION

1. Polymer Pre-processing

Small batches of SMP-10 were pre-processed to induce mass loss prior to mixing with SiC powders, in order to minimize mass loss and shrinkage after curing and sintering. Significant mass loss (>10 wt%) can be induced under heat and vacuum without initiating polymer curing at temperatures up to 90°C [24]. Pre-curing was tested under multiple conditions in order to determine an optimum heating time to maximize mass loss without inducing curing. Initial trials included venting SMP-10 in a beaker under a fume hood. Airing SMP-10 at room temperature for 24 hours produced negligible (~1%) mass loss. The beaker was then heated for four hours over a hot plate so that the surface temperature of the SMP-10 in the beaker was between 75–105°C when viewed with a FLIR infrared (IR) camera. Since this caused a cured layer to form at the surface of the SMP-10 in the beaker, a magnetic stirrer was added and the trial was repeated, with increasing temperatures, in an attempt to determine the best pre-curing heating profile. These approaches were not satisfactory as they have not produced significant mass loss, as compared to prior work, without curing the polymer.

Subsequent approaches were conducted with small (<1g) samples of SMP-10, with heating conducted under vacuum using an Accutemp-09 Series 480-degree F (Maximum

rated temperature of 248.8°C) Vacuum Oven (VAO) by Across International (Figure 18). Later SMP-10 preparation was conducted with 5–10 gram samples, which proved to produce more consistent and predictable mass loss percentages (~7-8% mass loss). Initially, optimized preparation consisted of heating SMP-10 samples at 90°C for 24 hours. However, as the stock SMP-10 aged over the course of this study, it began to gel and thicken noticeably at room temperature within its original container. Therefore, the pre-curing was performed under vacuum at 70°C for 18 hours for all the final samples that are presented.

Figure 18. Vacuum Oven (VAO)

2. Sample Mixing

Solids loading of the heat-treated SMP-10 was conducted at percentages varying from 80 wt.% powder to 20 wt.% polymer (80/20) to 84/16. This was done to maximize solids loading while keeping the viscosity manageable. Samples of 18–25g were prepared in 50 mL FlackTek mixing cups. Mixing was conducted using a FlackTek, Inc. Speedmixer™ (Model# DAC 150.1 FVZ-K) (Figure 19).

Figure 19. Flacktek Speed Mixer

Mixing regimens initially consisted of two rounds of one-minute cycles at 1,200 revolutions per minute (RPM) with hand mixing in between to remove stuck material from the corners of the containers, followed by a 15 second cycle at 3,000 RPM. The overall procedure was then repeated once more. It was determined that the mixing cycles at 3,000 RPM produced a significant amount of heat in the mixed sample, which in turn began to cure the SMP-10 during mixing, causing the mixtures to thicken. At this point, mixing cycles at 3,000 RPM were reduced to 5 seconds with a one-minute cooling period. Post-mixed samples were weighed for density by filling a silicone cube mold with an edge length of 10 mm. It was determined that samples mixed under normal atmospheric conditions included a significant amount of trapped air, up to 10 vol.%. After being weighed, samples were re-mixed (using the same mixing regimen) under vacuum and weighed, showing a nearly 10% increase in density. All samples were subsequently mixed solely under vacuum. This was achieved by placing the mixing cup (without lid) into a special mixing cup holder (Figure 20). The lid for the holder contains a one-way valve which is connected to a vacuum pump. The samples were evacuated for 30 seconds.

Figure 20. Standard FlackTek 50 mL Container Holder (left) and 50 mL Container Holder for Vacuum Mixing (right)

3. Molding and 3D Printing

Initial attempts to mold cubes (6 mm x 6 mm x 6 mm) used natural clay or Sculpey® polymer clay molds, but cured parts could not be removed from the molds without destroying the parts. Subsequently, small cubes (10 mm x 10 mm x 10 mm) were molded by hand-packing mixed material into a commercially available silicone ice cube tray (Figure 21). This was also used to determine the density of the material, directly measured as g/cm^3.

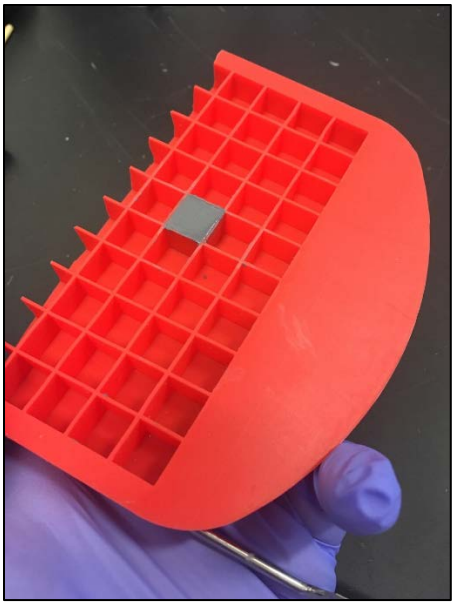

Figure 21. Silicone Mold (1 cm^3)

Initial samples were 3D printed using a Monoprice MP Mini Delta 3D Printer modified for VAP (Figure 22). Syringes with nozzle sizes of 0.5-0.6 mm were packed with approximately 5–8 grams of mixed material, then connected to a source of compressed air, with pressure varying from 69–760 kPa, depending on the viscosity of the mixed material. The samples were printed onto glass slides (used to transfer the printed material for curing) at a rate of up to 10 mm/s with layer heights of 0.2-0.3 mm. To reduce material deformation and creep at the bottom of the parts during printing, the printer base was modified with a thermoelectric heating/cooling element to print onto a cold plate (0-5°C). Similarly, printing was also conducted using a hot plate at 90–150°C in order to reduce creep during printing by partially curing the material as it printed.

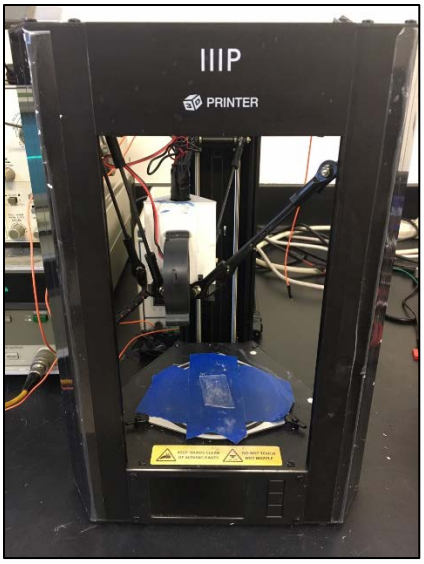

Figure 22. Monoprice MP Mini Delta 3D Printer Modified for VAP

Samples were later 3D printed with a Monoprice MP Inventor I Fully Enclosed Dual Extruder 230 3D Printer (Figure 23), with one of the extruders modified for VAP. The printer allowed for the simultaneous printing of thermoplastic support material in concert with VAP of SiC mixed material. The slicing was done using the Simplify3D software and a custom python code to modify the generated gcode for VAP.

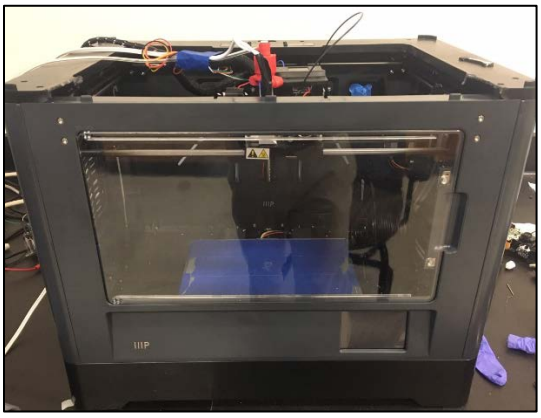

Figure 23. Monoprice MP Inventor I Fully Enclosed Dual Extruder 230 3D Printer Modified for VAP

4. Sample Curing

All molded and printed samples were cured using the VAO. Initially, samples were cured in two stages: the first stage consisted of 10 hours under normal (~1 atm) pressure at 100°C, followed by a second stage of three hours under vacuum at 248.8°C [22]. Samples were removed from the mold or glass slide (as applicable) between the two stages. The curing process was refined and samples were subsequently cured in three stages: (1) four hours under normal pressure at 80°C, (2) four hours under vacuum at 100°C, (3) four hours under vacuum at 248.8°C. This was due to the break-up of samples during pyrolysis, which indicates incomplete curing, as well as to minimize part expansion during curing. The four hours for each stage appeared to be sufficient for a depth of 6.35 mm from any surface of the sample and larger samples need proportionally longer curing durations (i.e., four hours per 6.35 mm).

5. Sample Pyrolysis

Samples were pyrolyzed using a Lindberg Blue M tube furnace by Thermo Scientific (Furnace Model STF54434C; Control Console Model CC59256PCOMC-1) (Figure 24). Initial samples were pyrolyzed under nitrogen flow of 1 L/min at a heating rate of 10°C/min from room temperature to 1600°C, followed by a one hour hold at 1600°C, which were then allowed to cool to room temperature [22]. Due to violent disaggregation of many of the samples and damage to the alumina tube, the heating schedule for pyrolysis was adjusted several times. Samples were pyrolyzed under nitrogen at a heating rate of 5°C/min from room temperature to 1600°C, a one hour hold at 1600°C, then cooled at a rate of 5°C/min to room temperature; however, samples continued to break up and cracking of the alumina tube was observed. Thermogravimetric analysis was used to inform additional adjustments. Samples were then heated at a rate of 2°C/min with a hold at 300°C for one hour, heated to 1300°C at 2°C/min and held for one hour before being cooled to room temperature at 2°C/min.

Figure 24. Lindberg Blue M Furnace Chamber and Control Console

Continued break up of samples during pyrolysis, along with increasing damage to alumina tubes, led to the use of a smaller Applied Test Systems 3210 Furnace with fused silica tubes (Figure 25) to view samples periodically during heating and determine the conditions (temperature, heating rate, etc.) where samples disaggregated.

Figure 25. Applied Test Systems 3210 Furnace

D. SAMPLE CHARACTERIZATION

1. Scanning Electron Microscopy

Molded and printed samples were analyzed before and after pyrolysis using a Zeiss Neon 40 Scanning Electron Microscope (SEM) (Figure 26) to determine the microstructure of each sample, including grain size and porosity. The SEM uses electrons to achieve image magnifications beyond 1,000,000X [32]. Electrons are first generated at the top of the column and accelerated downward toward the sample, where the electron beam is focused onto the sample through an aperture [33]. The electron beam is controlled using a raster over the sample with scan coils [33]. The electrons from the focused beam collide and interact with the surface of the sample and produce secondary and backscatter electrons, as well as characteristic x-rays [33]. Detectors for secondary and backscatter electrons collect and analyze these electrons, where an image of the material surface is produced [34]. Images of SiC samples were generated with 5–20 kV beam energy and 30–60 µm aperture sizes. Images were captured at magnifications from 36X to 2000X.

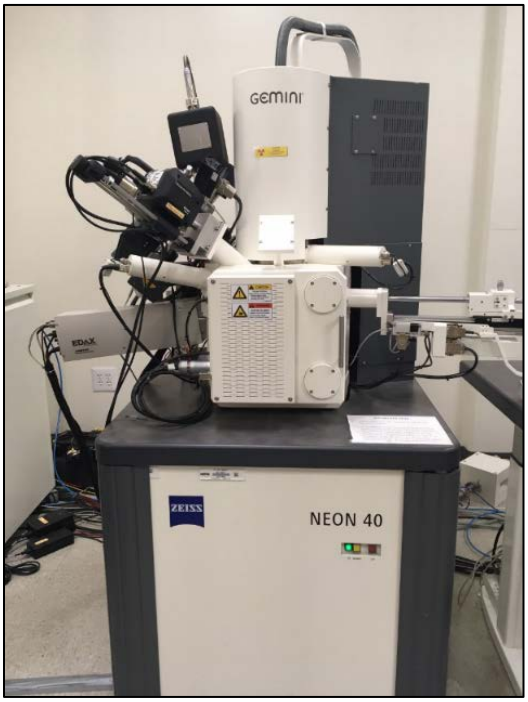

Figure 26. Zeiss Neon 40 SEM

2. Electron Dispersive X-ray Spectroscopy

Used in conjunction with the Zeiss SEM was an EDAX Pegasus Electron Dispersive X-ray Spectroscope (EDS). While within the SEM, atoms at the surface of the sample are excited by the electron beam and emit specific x-rays [35]. The emitted x-rays are characteristic of the atomic structure of the elements within the sample [35]. Analysis of the emitted x-rays is conducted using an energy-dispersive detector which is able to discriminate between the x-ray energies [35].

After images were captured with the SEM, the EDS was used with the same settings used to capture the SEM image, plus the high-current setting enabled. Resulting were spectra rendered for specified areas within the captured imagery. The spectra were analyzed using a database within the EDS software to determine the elemental breakdown of the materials in the sample. The breakdown would determine the stoichiometric ratio of silicon-to-carbon, as well as any impurities on the surface of the samples.

3. Particle Size Analysis

SiC powder was analyzed using a Horiba LA-950V2 particle size distribution analyzer (Figure 27). Using short-wave light and long-wave laser sources, this system can measure particle sizes ranging from 10 nm to 3 mm [36]. The system operates on the principle that light will scatter at angles dependent on particle size—smaller particles will scatter at wider angles than larger particles [36]. Analysis begins with two light sources of differing wavelength (which allows for wider detection limits), where light is scattered from interaction with suspended particles and collected by an array of photodiodes and subsequently analyzed using Mie Theory [36]. In this setup, powder samples were suspended in distilled water. Measurements were used to validate labeled particle sizes and their suitability for use in syringe nozzle sizes with an opening of 0.6 mm used within VAP.

Figure 27. Horiba LA-950V2 Particle Size Distribution Analyzer

4. Thermogravimetric Analysis/Differential Scanning Calorimetry

Thermogravimetric Analysis and Differential Scanning Calorimetry (TGA/DSC) of cured samples was conducted using a Netzsch STA 449 F3 Jupiter (Figure 28), which can measure mass changes and heat flow from ambient temperatures up to 1600°C [37]. TGA entails the continuous measurement of a sample's mass as the sample is heated under set heating conditions in order to observe mass loss or gain [38]. Similarly, DSC is used to measure the heat flow for a sample against a specified temperature range under a controlled atmosphere [39]. The change in heat flux of a container with a sample is compared to that of an empty container during the measurement, in order to deduce the change in heat flux due to the sample releasing or absorbing heat [39]. DSC measurements can be used to quantify the enthalpy of specific transitions such as glass transition, melting, crystallization, and chemical reactions [40].

Two samples ~20 mg each were analyzed by using TGA/DSC under argon flow at 100 mL/min from 30°C to target temperatures of 1150°C and 1400°C, at a rate of 2°C/min. Post-processed (now pyrolyzed) samples were saved for subsequent analysis. Mass-versus-temperature profiles were used to refine pyrolysis procedures, as discussed in section C5 of this chapter.

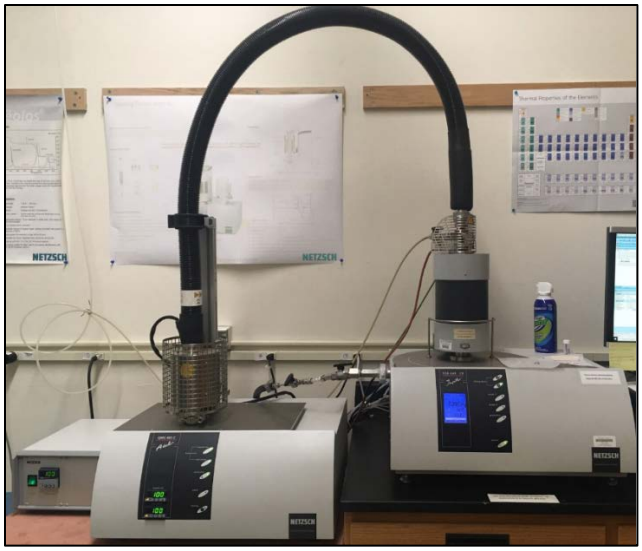

Figure 28. Netzsch STA 449 F3 Jupiter TGA/DSC

5. X-ray Diffraction

SiC powder, as well as pyrolyzed samples, were analyzed using a Rigaku Miniflex 600 X-ray Diffractometer (XRD) (Figure 29), a benchtop x-ray diffraction analyzer which operates with a 600 W x-ray tube [41]. Using a diffractometer, the diffracted intensities are detected, as a function of the angle of incidence [42]. A spike in intensity correlates to constructive interference of diffracted x-rays, which allows the measurement of spacing between crystal planes in the sample (illustrated in Figure 30), using Bragg's Law

$$n\lambda = 2d\sin\theta \ , \tag{1}$$

where n is the order of reflection, λ is the beam wavelength, d is the characteristic spacing of the crystal planes, and θ is the angle of incidence of the x-ray beam [42].

Figure 29. Rigaku Miniflex 600 X-ray Diffractometer

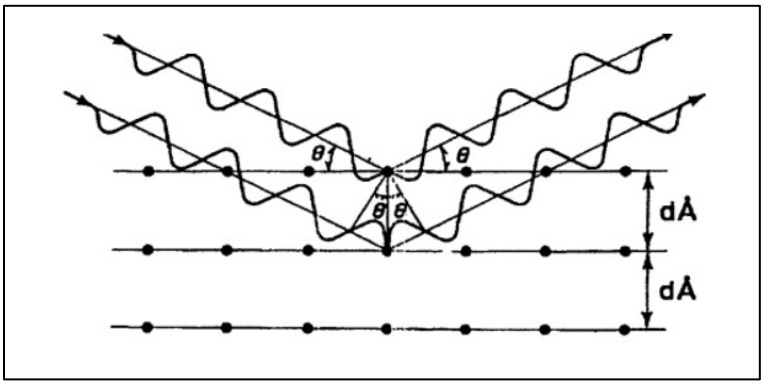

Figure 30. X-ray Diffraction by Crystal Planes. Source: [42]

When compared with available reference Joint Committee of Powder Diffraction Files (JCPDF) data, the crystalline structures of samples were determined and compared with each other. Post-processed samples from TGA were also analyzed with the XRD and compared to each other. Additionally, pre-processed SiC powder was analyzed to determine its crystalline phase. All samples were analyzed for diffraction angles of 10 to 90 degrees (2θ) with a step size of 0.01 degree at 10 deg/min.

6. Compression Testing

Compression testing of pyrolyzed cube samples was conducted using a Bluehill Universal Instron Compression Tester (Figure 31). Sample sizes were measured using a micrometer before being crushed in the compression tester. Data yielded the force applied with associated displacement. The data was used to determine mechanical (compressive) strength of the samples in the form of a stress-versus-strain plot.

Figure 31. Bluehill Universal Instron Compression Tester

III. RESULTS AND DISCUSSION

Beginning with testing feasibility of the ceramic TPS sandwich concept via computer simulation, the process of developing, building, and testing a small TPS sandwich tile consists of experimenting through many variables across several stages. Table 2 provides a summary of variables and considerations explored in this work, supported by details throughout this chapter.

Table 2. Summary of Variables and Considerations

Section	Variables	Considerations
Modeling and Simulation	Graphite middle layer vs. no graphite middle layer	With a constant heat load over time (up to 5 min), does a graphite middle layer improve TPS characteristics by effectively redistributing heat?
Polymer Pre-processing and Mass Loss	Temperature, time, pressure, sample size	What combination of temperature, heating time, and sample size will consistently produce ample mass loss (>6%) without curing the SMP-10?
Particle Size Analysis	SiC powder particles	Is particle size distribution within the SiC powder sufficiently small for VAP application?
Material Mixing	SiC powder/SMP-10 ratio, mix speed, mix time, pressure	What mixture ratio and mixing regimen produce optimized viscosity for VAP?
Molding and 3D Printing	Mold material, print bed temperature, dual extrusion printing with thermoplastics	What is the best material/method to use for molding SiC parts? Can print creep be reduced with: (1) a cold or hot print bed during VAP? (2) With a thermoplastic outer shell (from dual extrusion)?
Curing and pyrolysis	Temperature, heat/cool rate, time, stages	What process of curing (number of stages, temperatures, and time at each temperature) and pyrolysis (heat/cool rate and hold temperatures) will produce a SiC ceramic part with minimal defects (e.g., cracks)?

Section	Variables	Considerations
Characterization	SEM, EDS, XRD, compression testing	Will SEM images show difference in cured SMP-10 with powder compared to a pyrolyzed ceramic? Will EDS show a stoichiometric ratio of SiC or any impurities? Will XRD show α-phase or β-phase crystalline structures? Will SiC parts exhibit compressive strength favorably compared to reference data? Will printed SiC parts exhibit compressive strength favorably compared to molded parts?
Printing TPS materials	Print bed material, TPS sandwich middle layer material, dual-extrusion printing	How can cured (but not yet pyrolyzed) parts be transferred for pyrolyzing without breaking the part? What thermoplastic filament will best produce a graphite middle layer upon pyrolyzing the TPS sandwich?

A. MODELING AND SIMULATION

The concept for a SiC sandwich TPS with a graphite middle layer was tested by performing a transient thermal analysis using NX 12.0 by Siemens. A section of the leading edge of a wing was modeled, as shown in Figure 16 (Chapter II, Section A), with SiC outer layers and a graphite inner layer. Simulation setup is discussed in further detail in Chapter II, with material properties denoted in Table 1. Figure 32 depicts graphical results after 6 seconds of applied heat load. At this point in the simulation, differences in thermal profile between the two models is subtle.

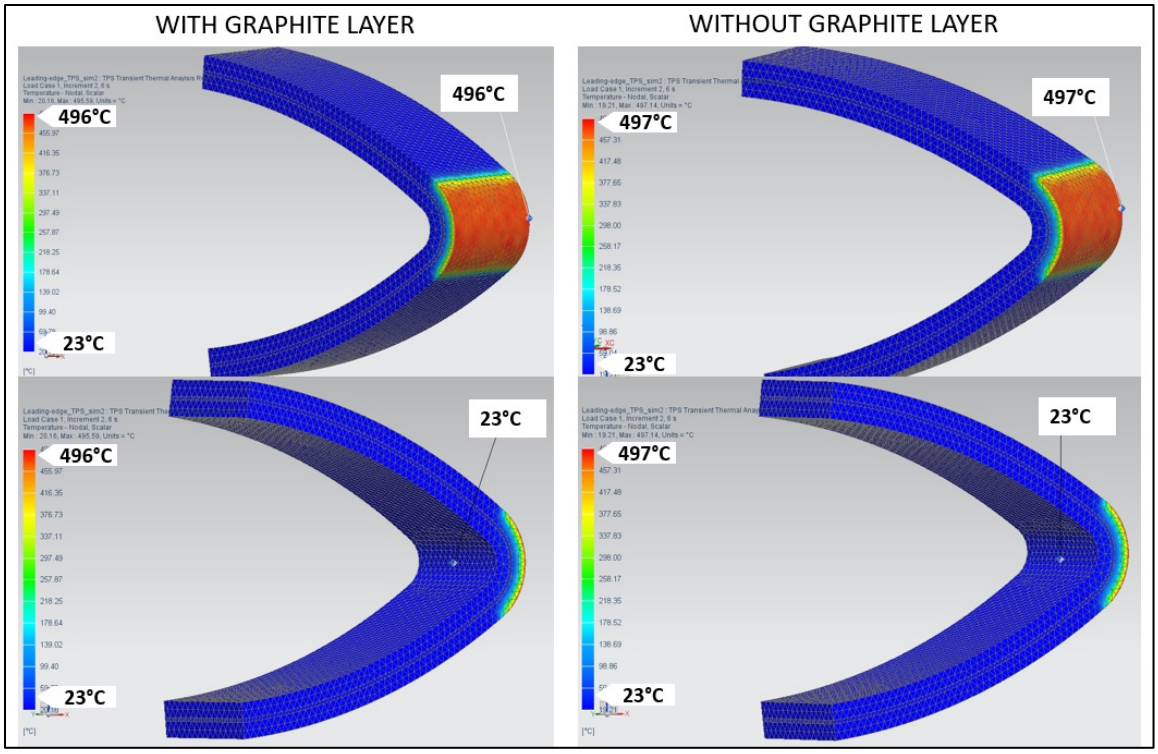

Figure 32. Simulated Comparison of TPS with Graphite Layer (left) and without Graphite Layer (right) at 6 Seconds

Comparative review of graphical simulation results shows that the two models diverge as simulation time increases. The view from the side shows that heat diffuses more slowly without graphite, since the graphite facilitates faster transfer of heat to cooler areas in the model. This effect becomes much more evident after 60 seconds of applied heat load, as shown in Figure 33. The surface of the inside of the wing without graphite also begins to show higher temperatures compared to the model with graphite.

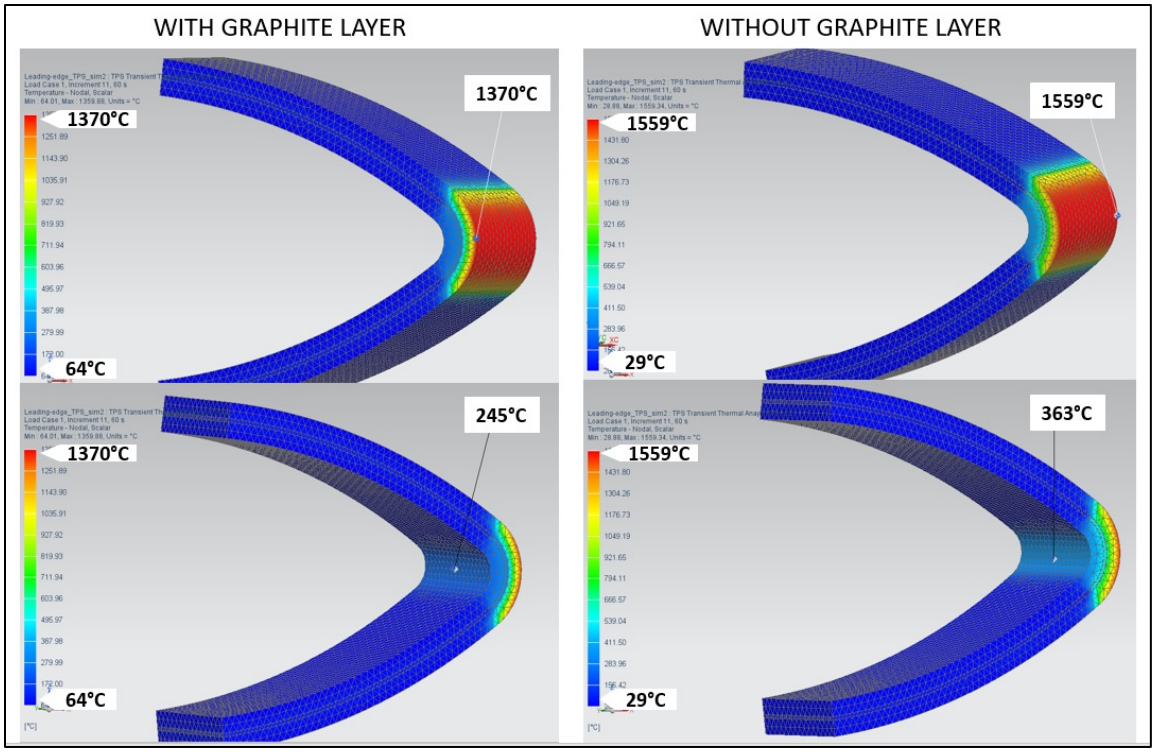

Figure 33. Simulated Comparison of TPS with Graphite Layer (left) and without Graphite Layer (right) at 60 Seconds

Transient thermal simulation was then extended to 120 seconds and 300 seconds in order to further analyze the divergence between the two models. The divergence is even more apparent at 300 seconds, as shown in Figure 34. Heating through the entire front of the wing, from the outer edge to the inner edge, is significantly higher without graphite, further showing the benefit of using a graphite layer to redistribute heat away from the thermal load.

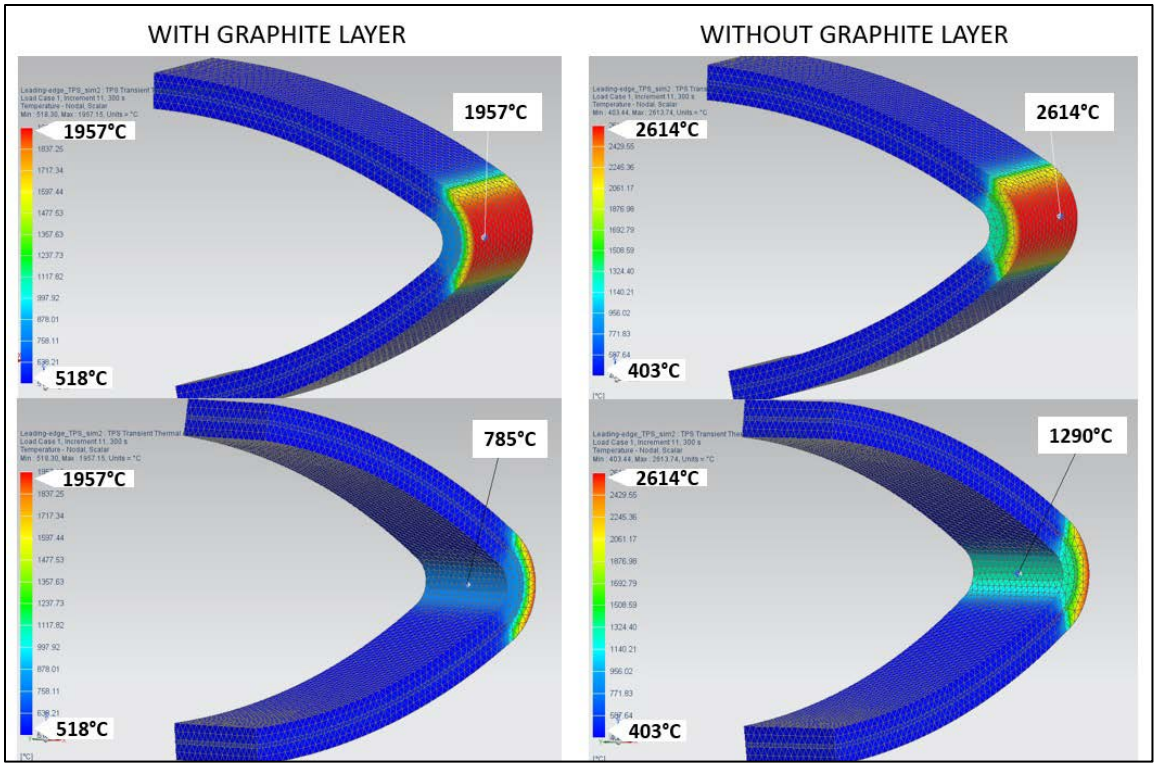

Figure 34. Simulated Comparison of TPS with Graphite Layer (left) and without Graphite Layer (right) at 300 Seconds

Analysis of data from the simulation was conducted by plotting maximum outer-surface and inner-surface temperatures over time for both models. Comparative results from the plots are shown in Figure 35. The divergence in the models over time is apparent on both outer and inner surfaces, which is significant for multiple reasons. After five minutes, the maximum temperature on the outer surface (where the heat load is applied) of the with-graphite model is more than 650°C cooler than a pure SiC model. Since the melting point of 6H-SiC is about 2,800°C [29], the temperature reduction from heat redistribution could significantly reduce TPS material degradation or allow harsher re-entry conditions, and even prevent catastrophic failure. Likewise, the inner surface of the model with graphite is more than 500°C cooler than the pure SiC model. This indicates that the structure with graphite is a more suitable TPS for protecting the surface of the spacecraft from extreme temperatures during atmospheric re-entry. This configuration would also have a lower density and overall weight at the same time.

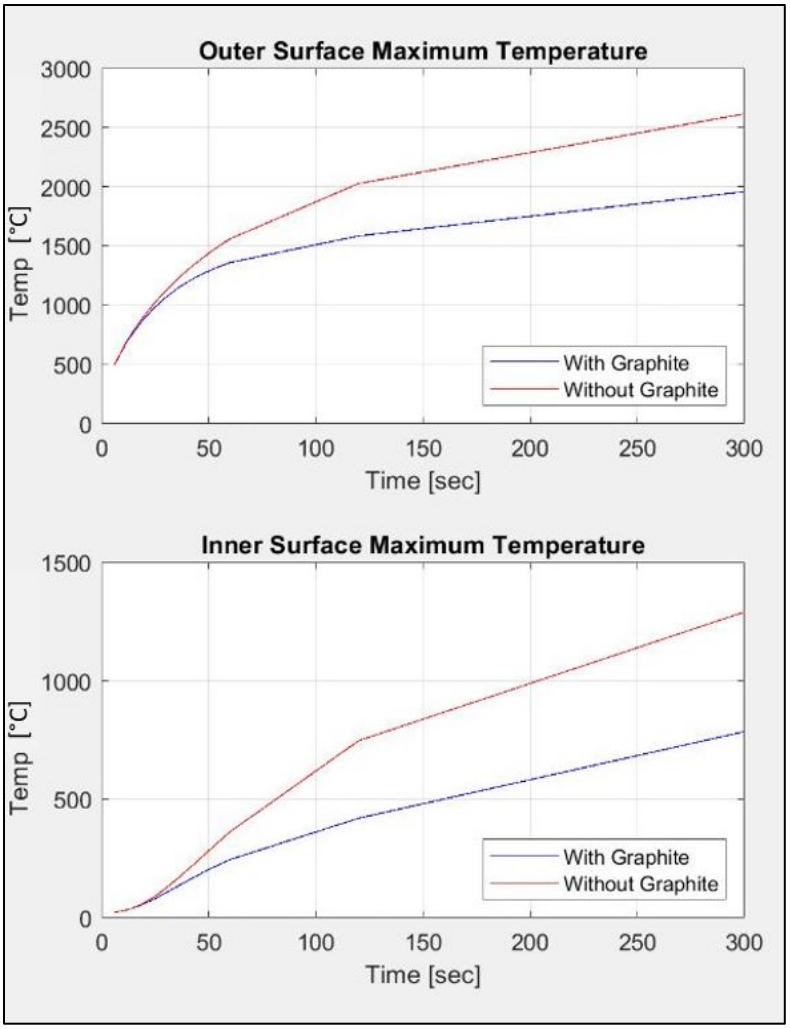

Figure 35. Simulated Comparison of TPS Inner and Outer Surface Maximum Temperatures with and without Graphite Layer

B. OPTIMIZATION OF MIXTURE FOR ADDITIVE MANUFACTURING

1. Polymer Pre-processing and Mass Loss

Various methods of pre-processing SMP-10 were explored in order to induce mass loss prior to mixing with SiC powder for VAP. Prior work showed that 10–14% mass loss of SMP-10 could be induced at an elevated temperature without curing the SMP-10 [24]. By inducing mass loss prior to the printing of parts, the extent of shrinkage and cracking during curing and pyrolysis can be reduced [22].

Initial attempts at reducing mass loss were conducted by placing the polymer in a beaker on a hot plate under a fume hood. The first trial included a small sample of SMP-10 (0.692 g) on a hot plate set at 90°C. A FLIR IR camera was used to measure the surface of the SMP-10 in the beaker, which was elevated to 75°C while on the hot plate. After 3.5 hours of heating, mass loss was measured at 8.2%. It was noted that a partially cured film had formed on the surface of the sample. Subsequent trials were conducted with a magnetic stirrer in larger sample sizes (~20 grams each). Additionally, a control sample of 3.021g was allowed to sit in a beaker at room temperature for 24 hours, where 1.3% mass loss was measured. The results of all SMP-10 pre-processing conducted in a beaker under a fume hood are summed up in Table 3, where reported temperatures denote the polymer surface temperatures, measured with the IR camera.

Table 3. SMP-10 Pre-processing in Open Beaker Under Fume Hood

Trial Description	**Initial Mass (g)**	**Polymer Surface Temp (°C)**	**Trial Time (hrs)**	**Final Mass (g)**	**Mass Loss (%)**
Hot Plate	0.692	75	3.5	0.635	8.2
Hot Plate + Mag Stirrer	20.0538	45	4	19.877	0.9
Hot Plate + Mag Stirrer	20.0657	75	4.5	19.6649	2.0
Hot Plate + Mag Stirrer	19.6649	75	4	19.27	2.0
Hot Plate + Mag Stirrer	20.102	77	4	19.5109	2.9
Hot Plate + Mag Stirrer	19.5109	105	4	18.987	2.7
Air @ Room Temp	3.021	Rm Temp	24	2.9825	1.3

In all the samples at or above 75°C, the formation of a thin, cured layer on the top surface was observed, which is believed to be due to the interactions with the ambient air. In order to better control applied temperatures and eliminate surface interactions/oxidation with air during heating, further SMP-10 pre-processing for mass loss was conducted using the vacuum oven. Trials began with small (~ 1 g) samples measured into 20 mL FlackTek sample cups. Samples were heated to 90°C under low vacuum using a single stage vacuum pump for various periods of time, and mass loss measured (see Table 4). Mass loss generally increased with heating time, but there was some sample-to-sample variation.

Table 4. 1-Gram Sample SMP-10 Pre-processing in Vacuum Oven

Initial Mass (g)	Temp (°C)	Trial Time (hrs)	Final Mass (g)	Mass Loss (%)	Notes
1.0462	90	1.2	0.9983	4.6	
1.0135	90	1	0.9408	7.2	
1.0401	90	2	0.9317	10.4	
1.0159	90	3	0.8957	11.8	
1.132	90	4	1.001	11.6	
1.134	90	4	0.999	11.9	
1.1741	90	6	1.0275	12.5	
1.1666	90	6	1.0251	12.1	
1.0228	90	8	0.9192	10.1	
1.1089	90	8	1.002	9.6	
1.0956	90	8	0.9911	9.5	
1.050	90	24	0.900	14.3	
1.020	90	48	0.852	16.5	Sample Gelled

To scale up the process, subsequent SMP-10 sample sizes were increased (~10 g) using larger FlackTek mixing cups (50 mL size cups), with the same pre-processing procedure under vacuum at 90°C. The first sample was removed from the oven and weighed at various intervals to measure the mass loss with time, as denoted in Table 5. Subsequent pre-processing of SMP-10 was then conducted under vacuum at 90°C (one sample at 85°C) for 24 hour periods, as denoted in Table 6. This method produced relatively consistent results. The mass loss in general was slower for 10 g samples compared to 1 g batches, thought to be due to the larger surface area per mass for the smaller samples that allows faster volatile removal.

It was also noticed that after approximately five months from initially opening the container of SMP-10, the container had partially collapsed and the stock SMP-10 had noticeably gelled, likely due to storing the material at room temperature without refrigeration. Since there was no means to determine the amount (if any) of mass loss within the stock material, pre-processing was then conducted with 10 g samples in 50 mL FlackTek cups under vacuum at 70°C for 18 hours (pre-processed sample shown in Figure 36), which is also recorded in Table 6. The mass loss fraction for these samples was lower by around 1–2 wt.%.

Table 5. Interval Mass Loss of 10 g SMP-10 Sample at 90°C

Initial Mass (g)	Interval (hrs)	Total Time (hrs)	Final Mass (g)	Interval Mass Loss (%)	Total Mass Loss (%)
10.0262	8	8	9.3876	6.4	6.4
9.3876	1	9	9.3143	0.8	7.2
9.3143	2	11	9.2093	1.1	8.3
9.2093	2	13	9.1283	0.9	9.2
9.1283	1	14	9.0693	0.6	9.8
9.0693	2	16	8.9873	0.9	10.7
8.9873	2	18	8.9203	0.7	11.5
8.9203	3	21	8.8933	0.3	11.8
8.8933	2.5	23.5	8.8453	0.5	12.3

Table 6. Larger Sample SMP-10 Pre-processing in Vacuum Oven

Initial Mass (g)	Temp (°C)	Trial Time (hrs)	Final Mass (g)	Mass Loss (%)	Notes
10.022	90	24	9.240	7.8	
10.018	90	24	9.261	7.6	
10.0032	90	24	9.163	8.4	
10.0139	90	24	9.1791	8.3	
10.028	90	24	9.2315	7.9	
10.044	90	24	9.2297	8.1	
10.031	85	24	9.139	8.9	
5.072	70	24	4.732	6.7	First @ 70°C
11.539	70	18.25	10.895	5.6	
10.601	70	18	9.976	5.9	

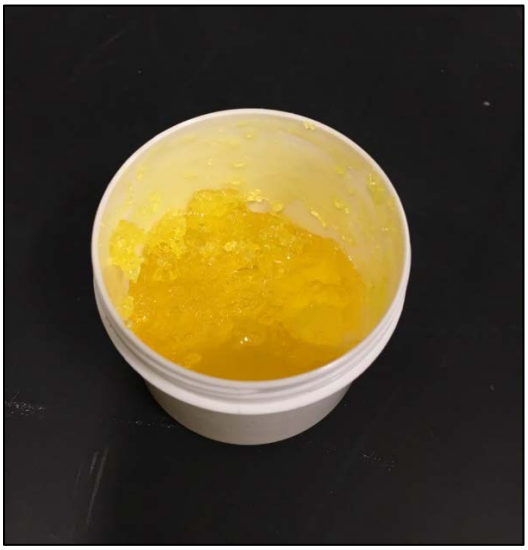

Figure 36. Pre-processed Sample of SMP-10 in 50 mL FlackTek Container

A graphical depiction of recorded mass losses (Figure 37) shows that mass loss percentage is generally more consistent and predictable with larger sample sizes during pre-processing of the polymer. Heating SMP-10 at 90°C under vacuum for 24 hours induced sizable mass loss and thickened the polymer for a more viscous, solid-loaded mixture (described in more detail in the next section) without curing of the polymer. Pre-processing the same size samples under vacuum at 70°C for 18 hours with the "age-thickened" SMP-10 also produced the same favorable processed polymer for mixing, albeit with a lower mass loss.

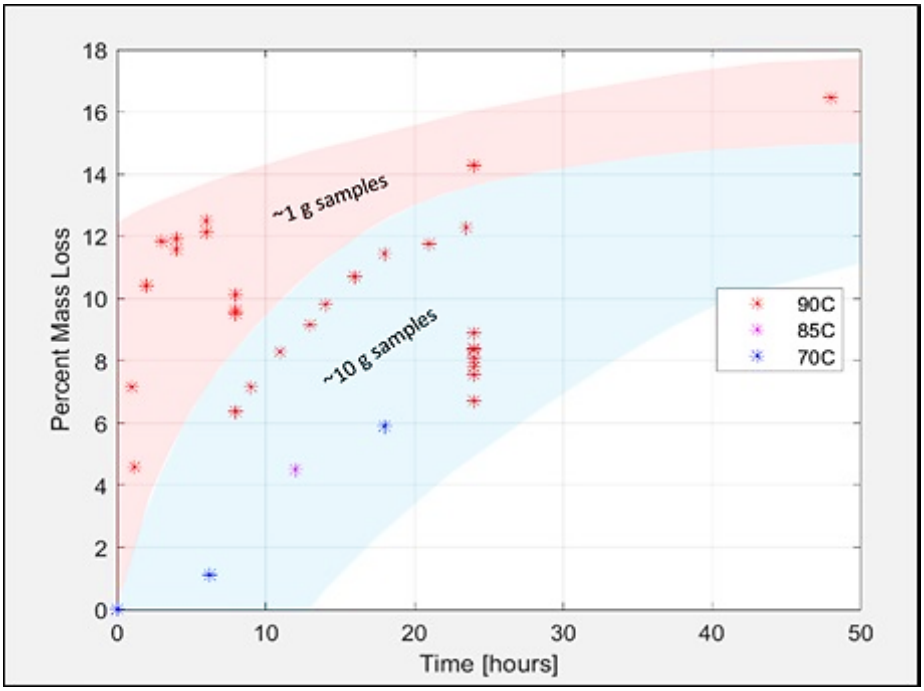

Figure 37. SMP-10 Pre-processing Mass Loss

2. Particle Size Analysis

Particle size analysis was conducted on the -400 mesh size (nominal mesh opening of 38 µm) SiC powder to determine its particle size distribution. As shown in Figure 38, all powder particles were under 80 µm, with a mean value of approximately 23 µm. Considering the nozzle diameter used for VAP is 600 µm, it was determined that the

particles within mixtures used for printing would not disrupt the flow of material during the printing process.

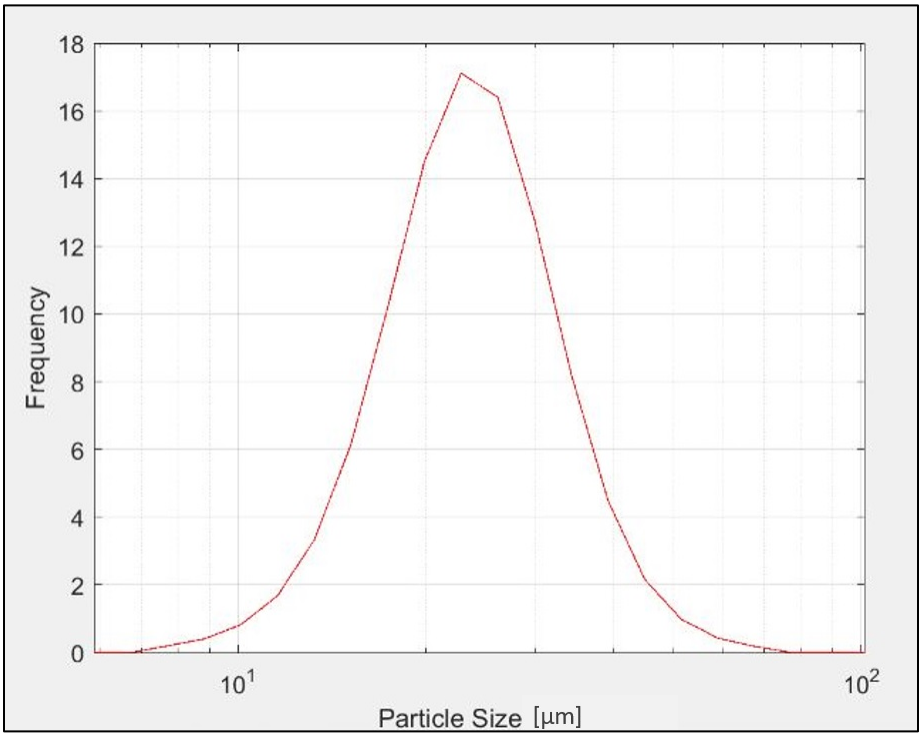

Figure 38. Particle Size Distribution for the -400 Mesh SiC Powder

3. Material Mixing

Pre-processed polymer was mixed with a high percentage of pure SiC powder to produce a highly viscous, “clay-like” mixture for VAP. Mixtures varied in powder wt. percentages from 80–84 wt.%. Mixing was also varied with mixing regimens of 1,200, 2,500, and 3,000 RPMs for varying amounts of time. Each mixture was tested by using VAP to print small test cubes (6 mm x 6 mm x 6 mm) and was generally either too soft (high amount of creep in printed parts) or too gritty (untenable flow or material break-up during printing). Initial mixtures are detailed in Table 7.

An additional factor in testing mixtures for printing were variations in printing techniques, discussed in further detail in the Sample Printing section. Lastly, while using the 1 cm^3 mold to estimate mixture density, it was determined that mixing under vacuum

increased the density of each mixture by approximately 10%; thus all subsequent mixtures were mixed under vacuum utilizing a special vacuum sealed sample holder for 50 mL FlackTek cups obtained from FlackTek. Cups (without lid) with sample mixtures were placed in the sample holder and connected to a single-stage vacuum pump. The sample holder was then evacuated for 30 seconds before being disconnected from the pump, then placed into the speed mixer. This effect was not observed when vacuum treatment was performed post-mixing, as the viscosity of the mixture is very high, preventing air removal.

Table 7. Initial Mixture with SiC Powder

Powder (g)	SMP-10 (g)	Mix Ratio (Powd/SMP)	Mix Regimen	Notes
4.018	1.051	80/20	Two cycles of: 1 min @ 1,200 RPM (x2) 15 sec @ 3,000 RPM (x2) 2 min @ 1,200 RPM	
16.034	4.006	80/20	1 min @ 1,200 RPM (x2) 15 sec @ 3,000 RPM w/ vacuum (x2) 2 min @ 1,200 RPM w/ vacuum	
20.25	4.75	81/19	1 min @ 1,200 RPM (x2) 15 sec @ 3,000 RPM w/ vacuum (x2) 2 min @ 1,200 RPM w/ vacuum	Mixture broke up in nozzle during VAP
20.25	4.993	80/20	1 min @ 1,200 RPM (x2) 15 sec @ 3,000 RPM w/ vacuum (x2) 2 min @ 1,200 RPM w/ vacuum	Pre-processed SMP-10 added to previous mixture
21.2912	5.0004	81/19	1 min @ 1,200 RPM (x2) 15 sec @ 3,000 RPM w/ vacuum (x2) 2 min @ 1,200 RPM w/ vacuum	
21.5352	5.0004	82/18	1 min @ 1,200 RPM (x2) 15 sec @ 3,000 RPM w/ vacuum (x2) 2 min @ 1,200 RPM w/ vacuum	Powder added to previous mixture
22.0082	5.0004	84/16	1 min @ 1,200 RPM (x2) 15 sec @ 3,000 RPM w/ vacuum (x2) 2 min @ 1,200 RPM w/ vacuum	Powder added to previous mixture

Powder (g)	SMP-10 (g)	Mix Ratio (Powd/SMP)	Mix Regimen	Notes
22.0082	5.2314	83/17	1 min @ 1,200 RPM (x2) 15 sec @ 3,000 RPM w/ vacuum (x2) 2 min @ 1,200 RPM w/ vacuum	Pre-processed SMP-10 added to previous mixture
24.558	5.03	83/17	1 min @ 1,200 RPM (x2) 15 sec @ 3,000 RPM w/ vacuum (x2) 2 min @ 1,200 RPM w/ vacuum 15 sec @ 3,000 RPM	
24.558	5.197	82.5/17.5	1 min @ 1,200 RPM (x2) 15 sec @ 3,000 RPM w/ vacuum (x2) 2 min @ 1,200 RPM w/ vacuum	Pre-processed SMP-10 added to previous mixture; mixture began to harden during mixing process
23.1663	4.9996	82.25/17.75	1 min @ 1,200 RPM (x2) 15 sec @ 3,000 RPM w/ vacuum (x2) 2 min @ 1,200 RPM w/ vacuum 15 sec @ 3,000 RPM	
21.647	4.752	82/18	1 min @ 1,200 RPM (x2) 15 sec @ 3,000 RPM w/ vacuum (x2) 2 min @ 1,200 RPM w/ vacuum 15 sec @ 3,000 RPM	
21.647	5.0797	81/19	1 min @ 1,200 RPM (x2) 15 sec @ 3,000 RPM w/ vacuum (x2) 2 min @ 1,200 RPM w/ vacuum 15 sec @ 3,000 RPM	

It was determined from the later mixing regimen listed in Table 7 that the mixed material was heating as a result of the particle friction during mixing, especially during the 3,000 RPM cycles. Therefore, subsequent mixing regimens reduced the time at 3,000 RPM from 15 seconds to 5 seconds, followed by a one-minute cool down period under a fan. Final optimized samples were made with “age-thickened” SMP-10 vacuum cured at 70°C for 18 hours, and then mixed with SiC powder at a solid loading of 80 wt.%, as shown in Table 8. Samples mixed at 1,200 RPM and 3,000 RPM are shown in Figure 39.

Table 8. Final SiC Powder/SMP-10 Mixtures

Powder (g)	SMP-10 (g)	Mix Ratio (Powd/SMP)	Mix Regimen	Notes
21.103	4.633	82/18	Two cycles of: 1 min @ 1,200 RPM (x2) under vacuum 5 sec @ 3,000 RPM under vacuum	Too viscous to print
19.688	4.902	80/20	Two cycles of: 1 min @ 1,200 RPM (x2) under vacuum 5 sec @ 3,000 RPM under vacuum	
18.291	4.580	80/20	Two cycles of: 1 min @ 1,200 RPM (x2) under vacuum 5 sec @ 3,000 RPM under vacuum	
15.420	3.855	80/20	Two cycles of: 1 min @ 1,200 RPM (x2) under vacuum 5 sec @ 3,000 RPM under vacuum	
19.468	4.865	80/20	Two cycles of: 1 min @ 1,200 RPM (x2) under vacuum 5 sec @ 3,000 RPM under vacuum	

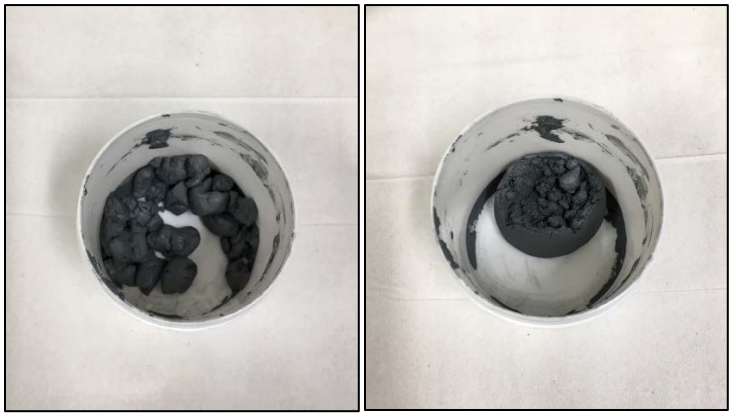

Figure 39. SiC Powder/SMP-10 Mixture after 1,200 RPM (left) and 3,000 RPM (right)

4. Molding and 3D Printing

Mixed material was used to create molded and 3D printed parts for characterization and testing. Initial molding was attempted with VAP-printed molds using natural clay or Sculpey® polymer clay. Upon curing of the SiC in the molds, however, the parts could not be removed from the molds without destroying the parts (Figure 40). Therefore, all molded parts were then produced using the 1 cm^3 silicone molding tray shown in Figure 20 (see Chapter II, Section C3). The molds were easily filled by hand using a small spatula and cured parts could be removed from the mold fully intact. The silicone rubber in the mold was also able to withstand the curing temperatures. Additionally, three small segments (~5 mm) of PLA were inserted into one molded cube in order to determine what (if any) negative effects would result during curing and pyrolysis.

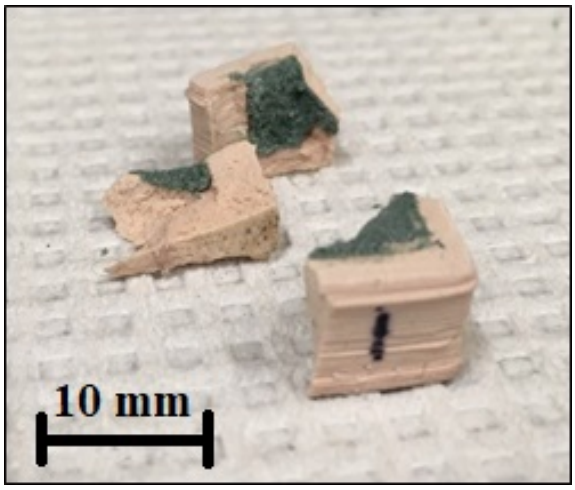

Figure 40. Part in VAP Printed Sculpey® Clay Mold

Initial printing of parts was conducted with a single extruder printer, adapted for VAP. Testing of material mixtures and printing techniques was conducted by printing simple 6 mm x 6 mm x 6 mm parts with a layer height of 0.2 mm. Early printed samples exhibited a large amount of creep, as shown in Figure 41. Print quality required optimization to reduce or prevent breakup in the nozzle, or creep in the part once printed.

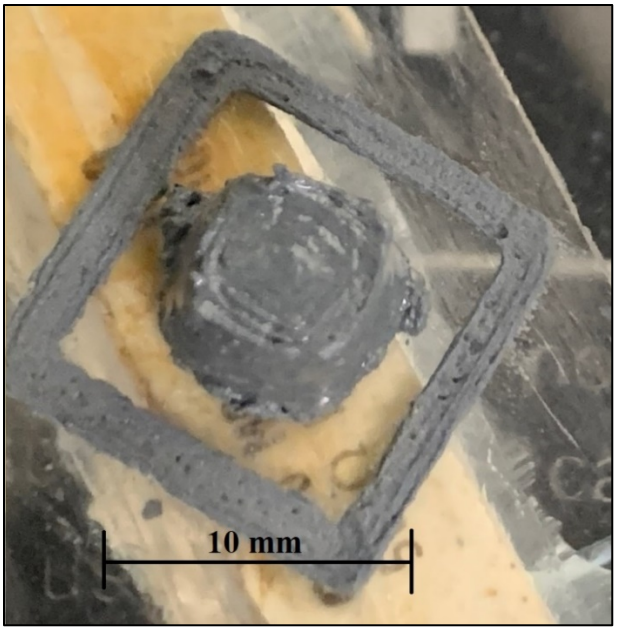

Figure 41. Printed Part with Creep

It was observed that material mixtures with nominal viscosity for VAP exhibited some degree of deformation and creep in printed parts. To reduce this effect, variations in printing bed temperatures were explored. First, a thermoelectric element plate on an aluminum heat sink was connected to a power supply and was attached to the print bed, underneath the glass slide that the part was to be printed on (Figure 42). The print surface was cooled to approximately 0–5°C, as measured with a FLIR IR camera, to cool and stiffen the printed material in-situ. However, the cold print bed at these temperatures did not eliminate part creep or otherwise improve printability.

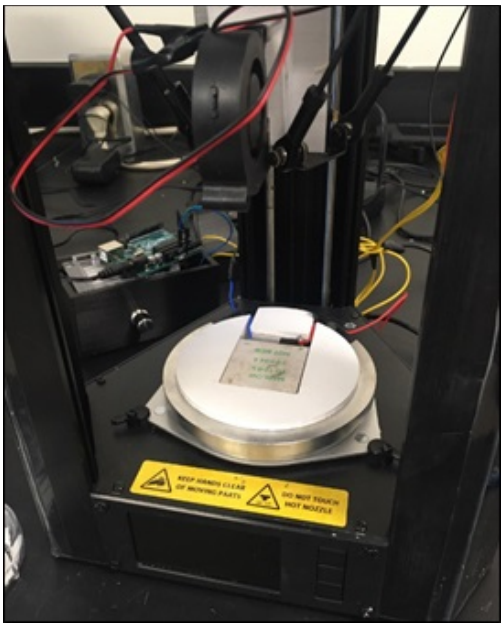

Figure 42. VAP Printer Fitted with Cold Plate Print Bed

The VAP printer was then fitted with a 50 Ohm resistive heating element on the print bed, with a glass slide fixed to the heating element using a zirconia ceramic paste for a removable print surface. This concept attempted to partially cure and harden the part on the print bed as it printed. Printing surface temperatures were varied between prints in an attempt to determine a nominal print condition. Temperatures ranged from 90–150°C, as measured with a FLIR camera. Successfully printed parts with minimal creep were produced (Figure 43), but could not be repeated without change to material viscosity, which usually resulted in the breakup of material in the print nozzle. It was postulated that this occurred due to the convective heat build-up in the print nozzle from the hot plate below, which caused the material to thicken over the print time. Pauses of up to 2 minutes were then added between layer prints in order to introduce nozzle cooling periods and to allow the printed section to cure longer, which drastically increased print time, but did not improve the overall print reliability for multiple parts.

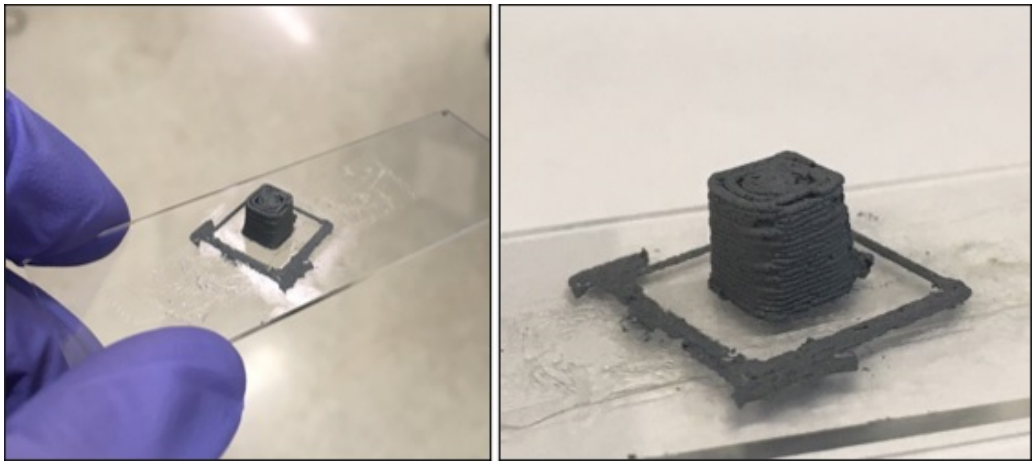

Figure 43. Successful SiC Test Print with VAP

The results of test prints using the single extruder printer showed that small SiC parts could be printed with VAP, but reliability in print quality was very limited with print height beyond 3 mm. The taller the part to be printed, the greater the chance of failure during printing. To mitigate this issue, a dual-extrusion print concept was explored. A dual-extruder printer was adapted for VAP for one of the extruders, while the other extruder remained unmodified (to print thermoplastics). The part was sliced to print the outer layers with PLA while VAP would be used to print the inner fill with a SiC mixture. The PLA (or another filament such as a water-soluble filament) serves as a support structure to reduce creep and ensure better part shape for taller prints. The concept resulted in successful test prints (Figure 44) and thus allowed for taller and more complex parts to be printed with a SiC mixture.

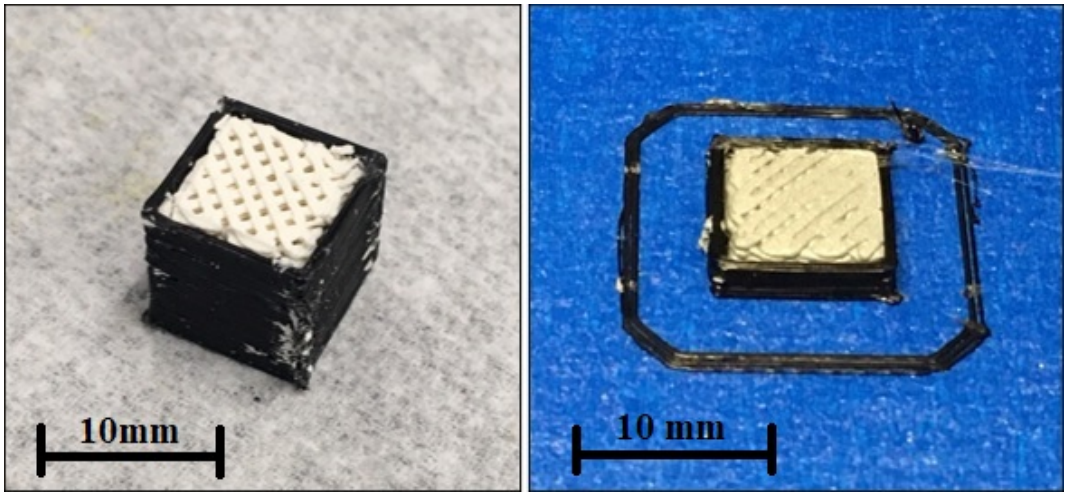

Figure 44. Successful Dual-Extruder Prints with Sculpey® Infill (left) and SiC Mixture Infill (right)

5. Curing and Pyrolysis

Molded and printed parts were cured through a series of heating cycles in the vacuum oven in order to harden mixed material through cross-linking of polymers and to volatize and expel carbosilane oligomers and hydrogen gas [22]. The first cured part, a 1 cm^3 molded cube, was placed in the vacuum oven under normal atmosphere at 130°C for one hour (the parts remained within the silicone mold tray during the first stage of curing). The part had hardened sufficiently to remove from the mold, but showed slight expansion along the top of the part and porosity along the sides resembling gas bubbles. Another molded 1 cm^3 cube was then placed in the oven under normal atmosphere at 100°C for one hour. Again, the part hardened sufficiently for removal from the mold, but rather than slight expansion, the top of the part exhibited a slight concave shape while the sides had far fewer pores. A comparison of the two cured parts is displayed in Figure 45 (note: the tops of the molds are facing the front in order to better view the porosity on the sides). The use of vacuum for this first stage caused samples to expand and was avoided.

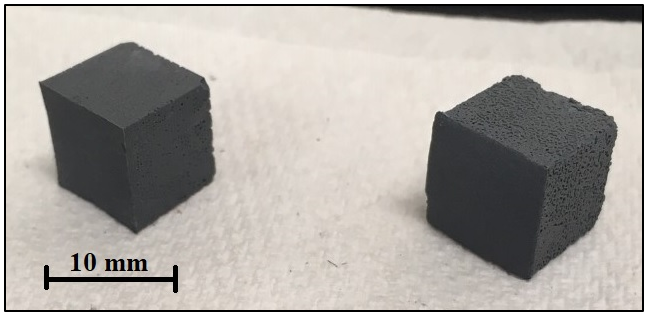

Figure 45. First Partial-Cure Molded Cubes at 100°C Initial Cure (left) and 130°C Initial Cure (right)

The second stage of curing initially consisted of a final round of heat curing of three hours at 248.8°C under vacuum, as referenced [22]. It was observed that the top surfaces of each of the parts formed cracks during the heating, likely due to the release of gases formed in the curing process. While both cubes formed cracks, the deformation was more apparent in the cube that was previously heated to 100°C for initial curing. Figure 46 shows the two molded cubes after the final curing stage.

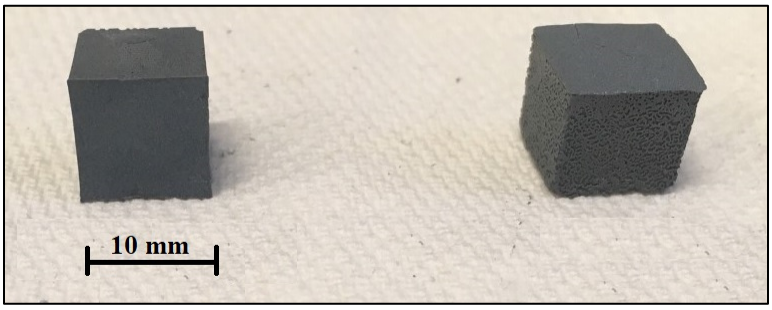

Figure 46. First Full Cure Molded Cubes at 100°C Initial Cure (left) and 130°C Initial Cure (right)

Subsequent parts (molded and printed) were cured in two stages: 10 hours at 100°C (no vacuum), followed by three hours at 248.8°C under vacuum, as referenced [22]. It was noted that the molded cubes exhibited slight expansion (<1 mm) during the curing process. Several parts, including the two molded parts already described, were pyrolyzed in a tube furnace under inert gas (N_2) from room temperature to 1,600°C at a ramp rate of 10°C/ min, and held at 1,600°C for one hour before returning to room temperature. All parts broke

apart during pyrolysis, with the exception of the two aforementioned molded cubes, one test print sample (6 mm x 6 mm x 6 mm), and the molded cube with PLA segments. The molded cube with PLA showed minor cracking, but remained mostly intact. The furnace alumina tube also cracked and had to be replaced.

The breakup of parts during pyrolysis was attributed to rapid mass loss and outgassing as the SMP-10 decomposed and went through phase changes toward crystalline SiC ceramic. This was addressed in two ways. First, to eliminate the potential of trapped gases or uncured SMP-10 in the parts at the beginning of pyrolysis, the curing process was updated to include three stages: (1) heating to 80°C for four hours (no vacuum), (2) heating to 100°C for four hours under vacuum, and (3) heating to 248.8°C for four hours under vacuum. Secondly, to determine if (and at what temperature/s) rapid mass loss occurred above 250°C, TGA/DSC analysis was conducted on small cured samples, with a 2°C/min ramp rate from 30–1,400°C, under argon gas. The TGA results (Figure 47) show significant mass losses beginning at about 360°C and at about 1,300°C. The overall mass loss was approximately 5 wt.%, which is significantly lower than reported values for pure SMP-10 (~30 wt.%) [24]. This is due to the fact that only 20% of the sample was SMP-10 and the pre-treatment of SMP-10 already caused a significant mass loss. The density difference between SMP-10 (0.998 g/cm3) [22] and SiC (3.2 g/cm3) [29], indicates that a 5 wt.% reduction translates to about 16 vol.% reduction. Since this shrinkage should occur within the polymer only, the printed parts can be expected to retain their original shape and dimensions and have relatively low porosity between particles upon pyrolysis. As a comparison, a sample solely made from as-received SMP-10 would lose more than 80 vol.% of its starting volume [22].

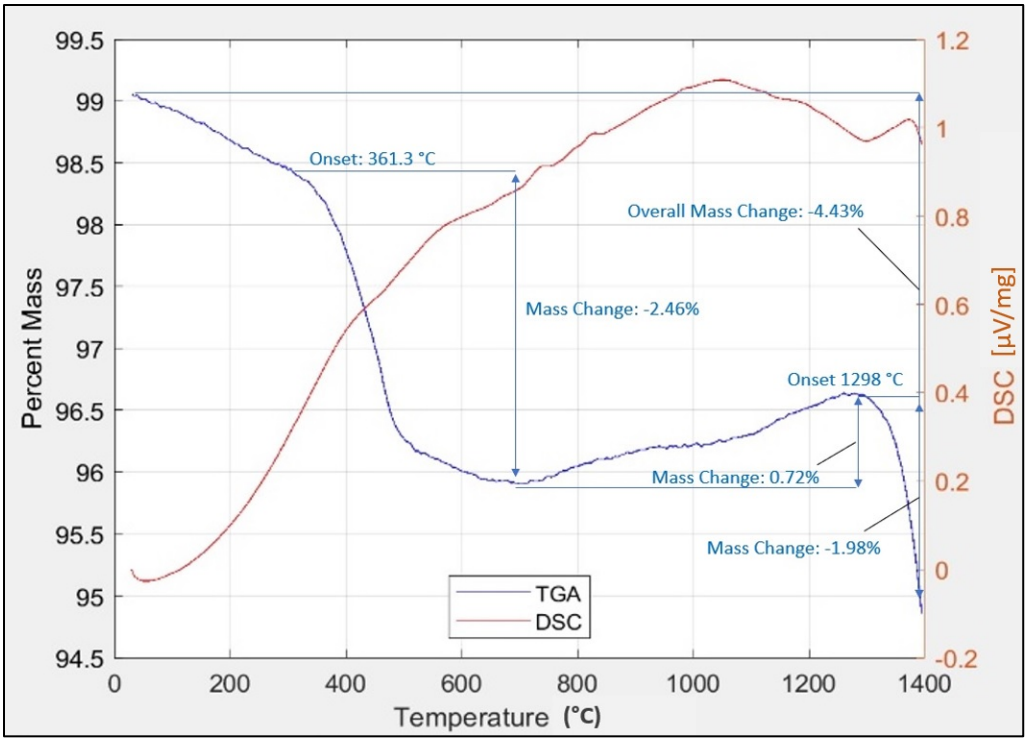

Figure 47. TGA/DSC of Cured SiC Sample

The pyrolysis process was adjusted and tested with more molded and cured parts. The adjusted process consisted of heating from room temperature to 300°C at a ramp rate of 2°C/min, with a hold at 300°C for one hour. The heating then continued to 1,300°C at a ramp rate of 2°C/min, with a hold at 1,300°C for one hour. Finally, the samples were cooled down to room temperature at a ramp rate 2°C/min. The parts broke apart during this process, though to a lesser degree than in the previous pyrolysis attempt. Figure 48 shows a pyrolyzed molded cube that broke apart mostly into two pieces. A slight differential in coloration at the center of the broken cube was attributed to the possibility that some of the SMP-10 may not have cured fully prior to pyrolysis.

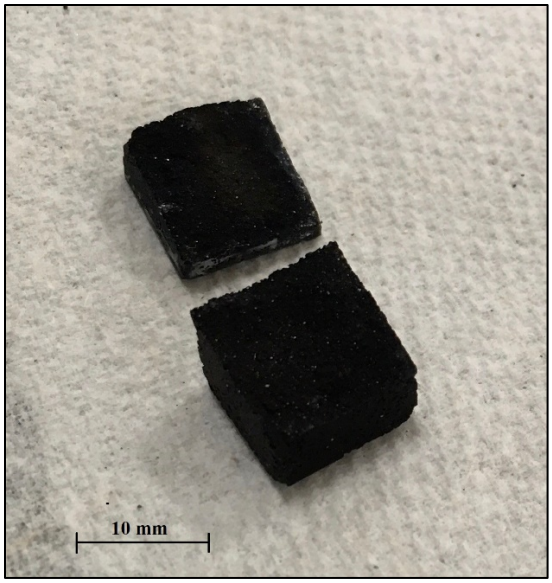

Figure 48. Breakup of Molded Cube During Pyrolysis

To better determine what temperature sample breakup was occurring, the smaller furnace with a clear, fused-silica tube was used to allow periodic observation of samples during pyrolysis (see Figure 25). Small, cured samples (pieces of molded samples and test prints) were placed into the furnace tube under inert gas (N_2), heated to a target temperature of 300°C and held at the target temperature for 30 minutes. Observing no change in the samples, the target temperature was set for 600°C with no control of ramp rate. At about 450°C, an audible crackling was heard, which was associated with the observed breakup of all samples in the furnace tube. After the furnace cooled, fresh cured samples were placed in the furnace tube under N_2 and heated to 355°C. After 10 minutes, the samples were heated to 475°C by increasing the temperature by 10°C every 5 minutes. No breakup of any of the samples was observed. The samples were then allowed to cool to room temperature and remained in the furnace tube. Approximately 72 hours later, the samples were re-heated under N_2 to 400°C. After 5 minutes, the samples were heated to 700°C by increasing the temperature 10°C every 5 minutes. The samples were then heated to 900°C by increasing the temperature 25°C every 3 minutes. No breakup of the samples was observed during this period of pyrolysis.

These results suggest that the part break-up is primarily due to the large mass loss and associated gas formation starting at ~350°C. Therefore, a longer hold time and slow heating rates can be effective in preventing the cracking and break-up of parts during pyrolysis.

6. Characterization of Materials

a. SEM

First, a SiC powder sample was analyzed to establish a baseline in particle size and shape. Images in Figure 49 show little variation in particle sizes, and correlates well with the particle size data (Figure 38). The particles appear to have jagged edges, typical for ceramics.

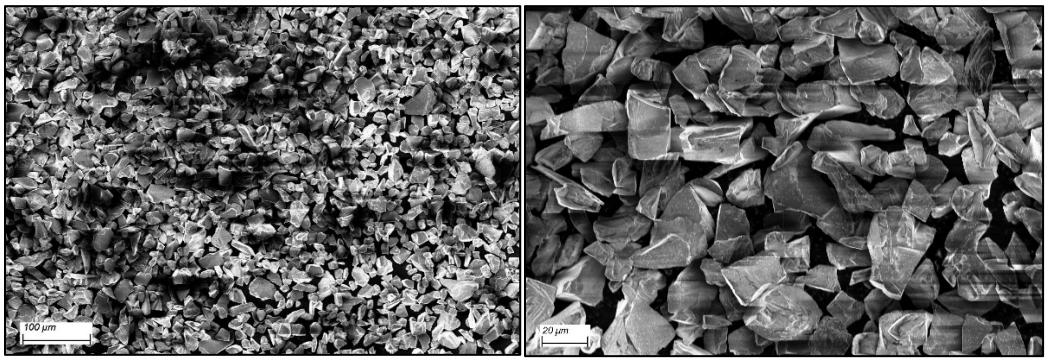

Figure 49. SEM Images of SiC Powder at 150X (left) and 500X (right)

SEM imaging was then conducted on parts that had been fully cured, but not yet pyrolyzed. A molded cube, fully cured up to 248.8°C, was analyzed at 200X magnification (Figure 50) and shows ceramic powder particles suspended in a matrix of hardened SMP-10.

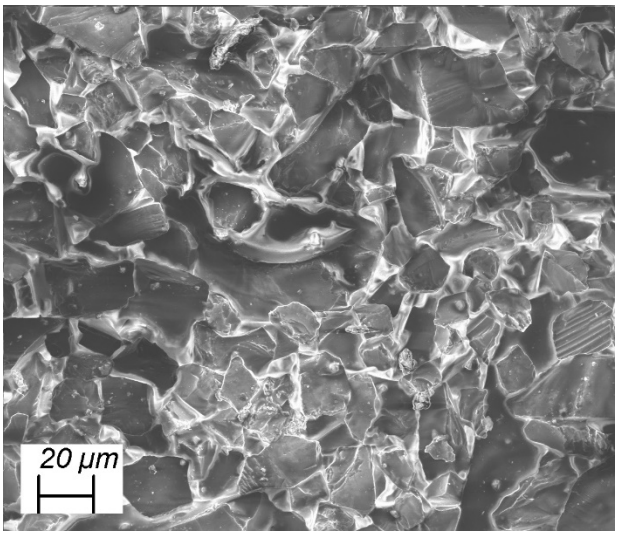

Figure 50. SEM Image of Cured Molded Part at 200X

Finally, pyrolyzed parts were analyzed to observe the transition of SMP-10 from a hardened polymer (Figure 50) to a ceramic crystalline structure (Figure 51). The molded cubes depicted in Figures 45 and 46 were analyzed after being pyrolyzed at 1,600°C; Figure 51 shows successive magnifications of 200, 500, 1,000, and 2,000X, with the left column images of the cube initially cured at 100°C and the right column images of the cube initially cured at 130°C. Since the surface of the cube on the left was initially much smoother (refer to Figures 45 and 46), the formation of a ceramic from SMP-10 appears much more apparent. Many fine cracks and pores are also visible on the surface as the pyrolyzed polymer decomposes and then shrinks to form the denser SiC. There were also some areas that showed the formation of nanorods on the surface. These were identified as silicon nitride (Si_3N_4) that formed as the samples reacted with the nitrogen gas during pyrolysis. The formation of silicon nitride from silicon carbide is reported elsewhere [43] and the reaction tends to be thermodynamically favored starting above 1450°C under nitrogen gas although not at significant rates up to 1,600°C [43]. For all of the samples, the extent of this reaction was limited to the surface only.

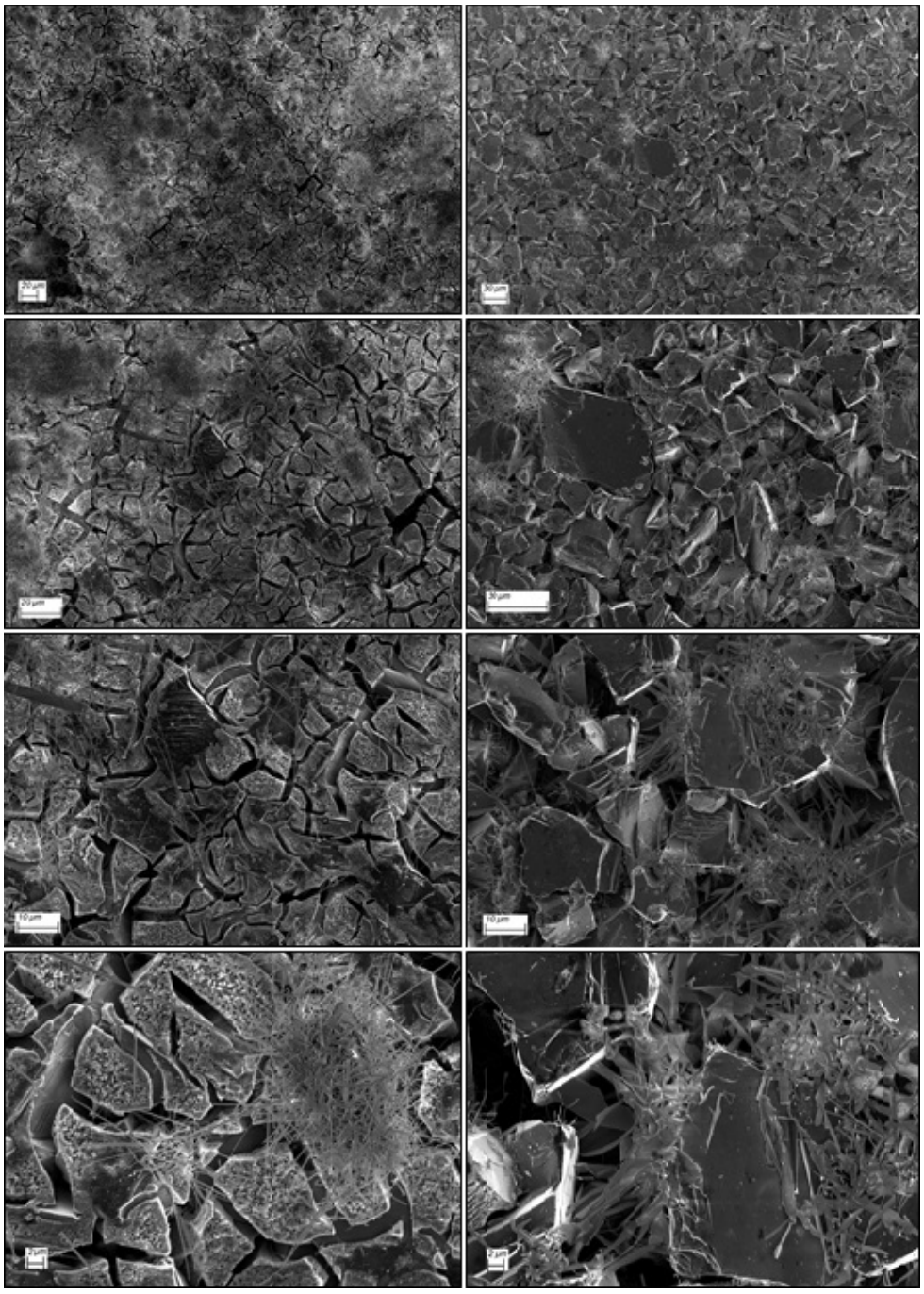

Figure 51. SEM Images of Pyrolyzed Cubes at 200X, 500X, 1,000X, and 2,000X

The pyrolyzed, molded cube with PLA segments was cut open in order to expose the PLA segments and examined with the SEM, as well (Figure 52). The molded cube did not break apart during pyrolysis, as did other molded cubes during the same period of pyrolysis, but did exhibit cracks. The PLA decomposed producing some gaseous products and possibly formed an amorphous carbonaceous char with a reduction in overall volume. This can be seen more clearly in the SEM images shown. Therefore, interfacing of these materials in the sandwich TPS should account for this to avoid cracking of the ceramic during pyrolysis (or use in re-entry). However, the results in general support the idea that suitable graphite forming polymers can be incorporated into these SiC structures by 3D printing.

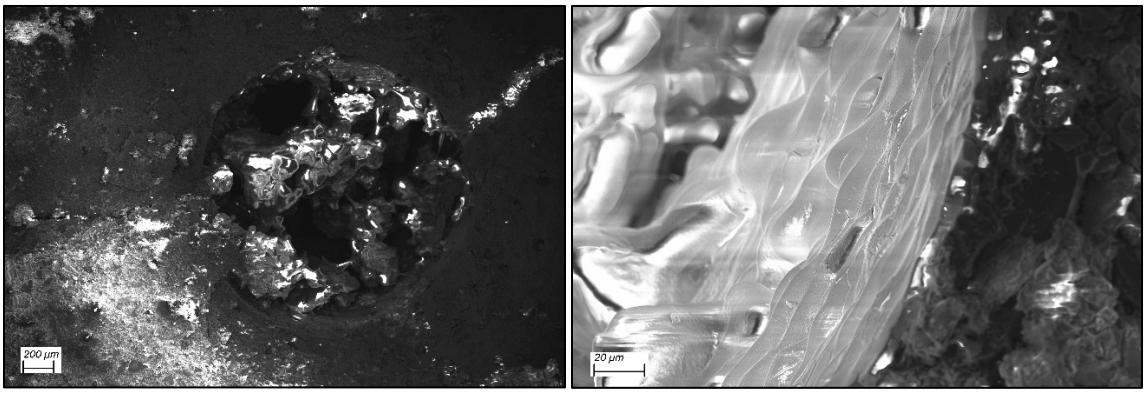

Figure 52. SEM Images of Pyrolyzed Molded Cube with PLA Segments at 30X (left) and 500X (right)

b. EDS

Used in conjunction with the SEM, the EDS was used to determine which elements were present in each sample, along with their relative quantities. Analysis was conducted on SiC powder (Figure 53), cured molded parts (Figure 54), and pyrolyzed parts (Figure 55). Figure 53 shows that the powder only contains silicon and carbon at a near-stoichiometric ratio. Of note, the x-ray spectra shown in Figure 53 is associated with Area 2 (light gray box) in the image shown.

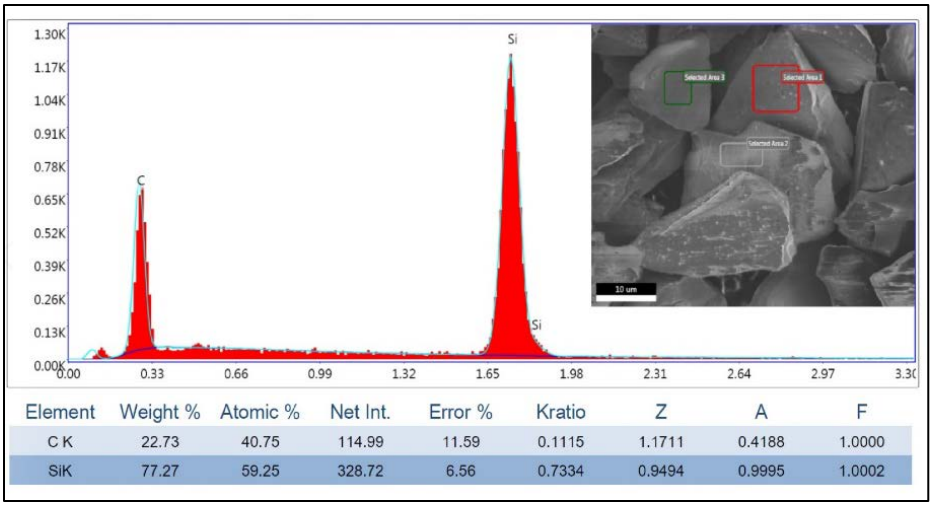

Element	Weight %	Atomic %	Net Int.	Error %	Kratio	Z	A	F
C K	22.73	40.75	114.99	11.59	0.1115	1.1711	0.4188	1.0000
SiK	77.27	59.25	328.72	6.56	0.7334	0.9494	0.9995	1.0002

Figure 53. EDS Spectra for SiC Powder

Cured, molded parts were analyzed with EDS and compared with the SiC powder EDS analysis results. Figure 54 shows the spectrum from EDS analysis of a molded part that was fully cured. A significant amount of oxygen was introduced into the sample surface since SMP-10 and the initial powders do not contain oxygen. This is likely due to oxidation during the first stage of the curing process, which cannot be done under vacuum without expanding the material in the mold. However, this can be done under an oxygen-free environment like argon or nitrogen at ambient pressure. Of note, the spectrum shown in Figure 51 corresponds to area 1 (red box) in the associated image.

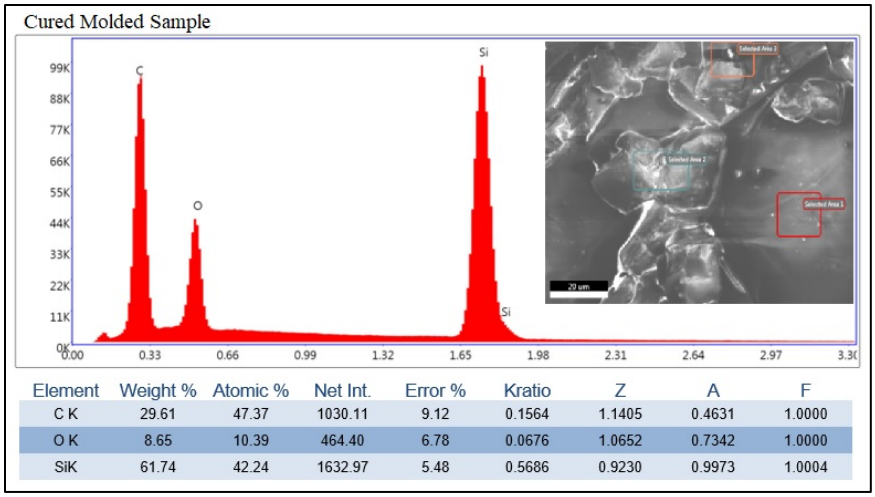

Element	Weight %	Atomic %	Net Int.	Error %	Kratio	Z	A	F
C K	29.61	47.37	1030.11	9.12	0.1564	1.1405	0.4631	1.0000
O K	8.65	10.39	464.40	6.78	0.0676	1.0652	0.7342	1.0000
SiK	61.74	42.24	1632.97	5.48	0.5686	0.9230	0.9973	1.0004

Figure 54. EDS Spectra for Cured Molded Part

EDS analysis of pyrolyzed samples included the molded cubes from Figures 45, 46, and 52. The spectra for both samples showed the formation of silicon nitride (Si_3N_4); however, the formations appeared relatively localized in smaller groups of nanorods with the 130°C initially cured cube. It is also important to note that these formations are on the surface of the pyrolyzed parts (from the N_2 environment during pyrolysis) and are not likely to exist within the interior of the parts in large quantities as they were not observed on fractured surfaces. This was not confirmed with additional EDS analysis during this research, but XRD results in the next section support this idea. Additional impurities were found, such as oxygen and aluminum. Figure 48 shows EDS spectra for the 100°C initially cured cube (top) and 130°C initially cured cube (bottom). Of note, the spectrum shown for the 100°C initially cured cube is associated with area 3 (orange box) in the image and the spectrum shown for the 130°C initially cured cube is associated with area 1 (red box) in the image.

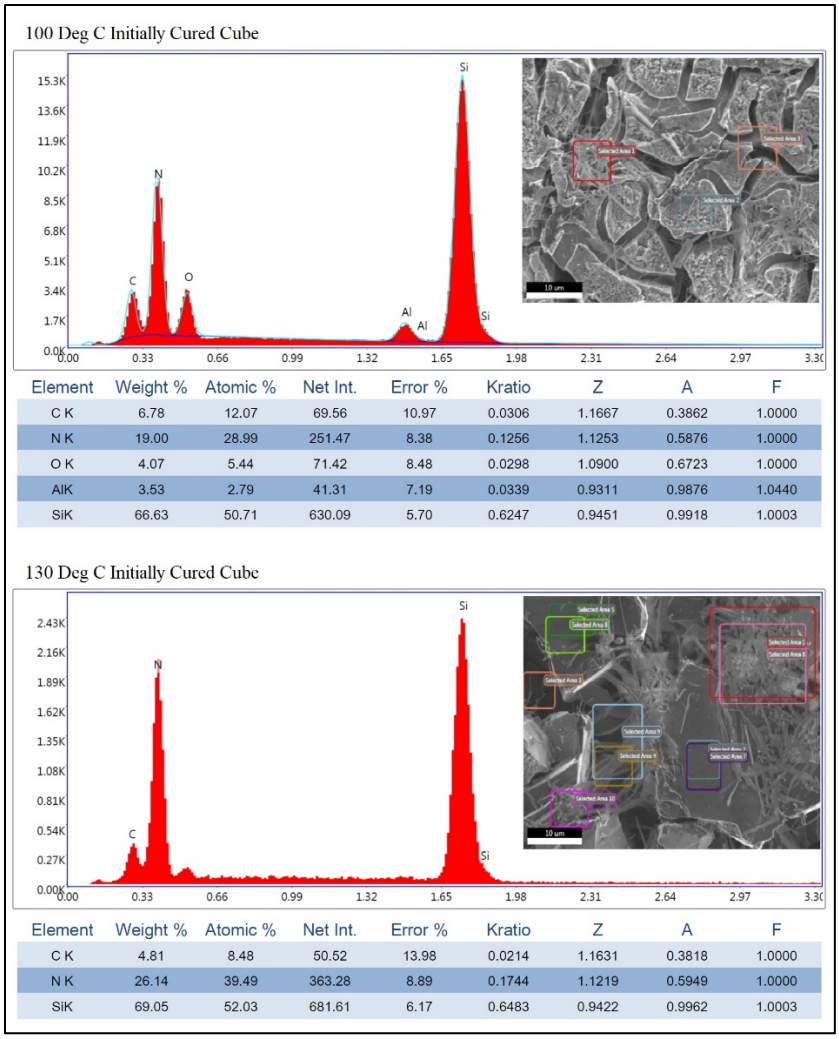

Element	Weight %	Atomic %	Net Int.	Error %	Kratio	Z	A	F
C K	6.78	12.07	69.56	10.97	0.0306	1.1667	0.3862	1.0000
N K	19.00	28.99	251.47	8.38	0.1256	1.1253	0.5876	1.0000
O K	4.07	5.44	71.42	8.48	0.0298	1.0900	0.6723	1.0000
AlK	3.53	2.79	41.31	7.19	0.0339	0.9311	0.9876	1.0440
SiK	66.63	50.71	630.09	5.70	0.6247	0.9451	0.9918	1.0003

Element	Weight %	Atomic %	Net Int.	Error %	Kratio	Z	A	F
C K	4.81	8.48	50.52	13.98	0.0214	1.1631	0.3818	1.0000
N K	26.14	39.49	363.28	8.89	0.1744	1.1219	0.5949	1.0000
SiK	69.05	52.03	681.61	6.17	0.6483	0.9422	0.9962	1.0003

Figure 55. EDS Spectra for 100°C Initially Cured Cube (top) and 130°C Initially Cured Cube (bottom)

c. XRD

XRD analysis was conducted on SiC powder, as well as a pyrolyzed, molded sample that was crushed to form a powder. Figure 56 provides a reference XRD diffraction pattern from the SiC powder and fit those for α-6H phase of SiC, according to the JCPDF [44].

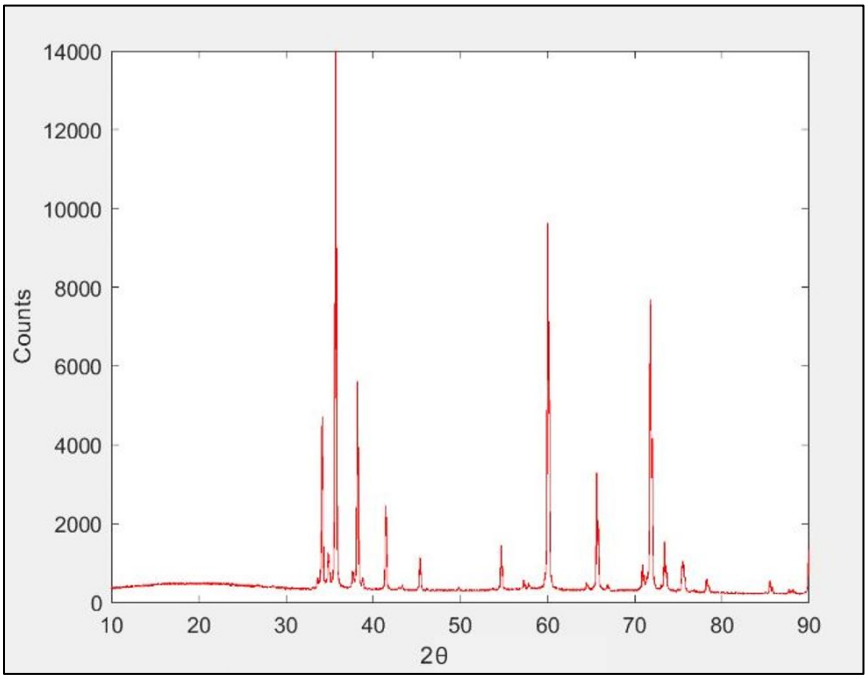

Figure 56. SiC Powder XRD Pattern

A molded sample, pyrolyzed at 1,300°C was also analyzed using XRD, with the resulting diffraction pattern shown in Figure 57, which favorably compares with Figure 56. Comparing Figure 57 with reference sources, the diffraction pattern indicates a 6H-SiC crystalline structure [44], [45], which is a well-known type of α-SiC [46]. The lack of a broad peak, characteristic of an amorphous structure, indicates the complete crystallization of the amorphous SiC phase that forms at lower pyrolysis temperatures [47].

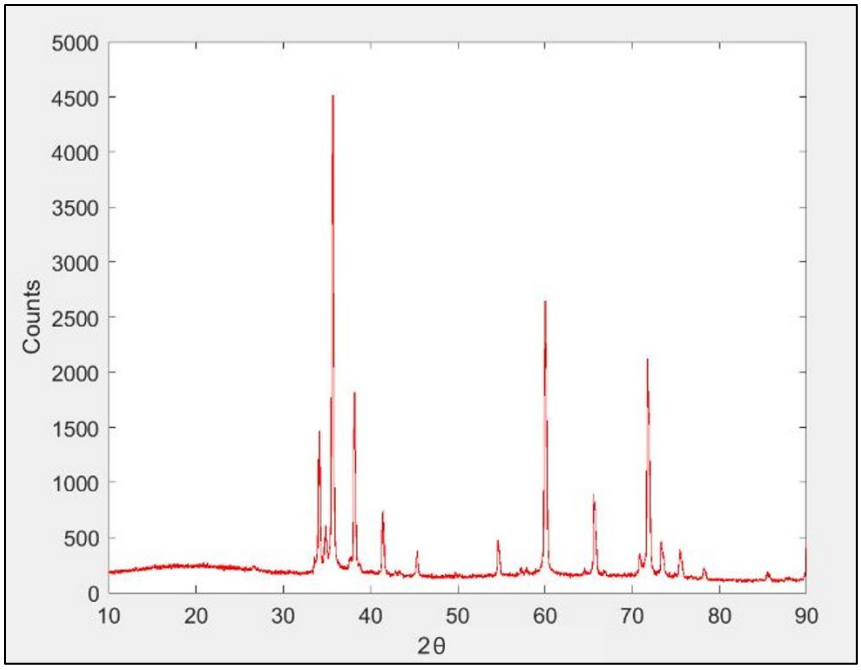

Figure 57. Pyrolyzed SiC Molded Part XRD Pattern

d. Compression Testing

Mechanical strength of a pyrolyzed cube was determined with compression testing. The cube chosen for testing was the 130°C initially pyrolyzed molded cube. Prior to crushing the cube in the machine, its physical dimensions (length x width x height) were measured with a micrometer: 10.14 mm x 10.14 mm x 10.08 mm. Testing parameters were set to crush the part at 2 mm/min. Data obtained included force applied with associated displacement, which was used to generate a stress-versus-strain plot (Figure 58). The plot shows that some displacement was observed prior to the maximum stress, which is likely associated with closure of small gaps from cracks developed during curing and pyrolysis. The maximum stress on the part was about 7.2 MPa, which was significantly lower than expected for a SiC ceramic part. Reference data shows SiC compression strength from 565–1,379 MPa [48] or even as high as 3,900 MPa [49]. The disparity is likely attributed to the part being weakened from cracks and voids formed during the non-optimum curing and pyrolysis processes.

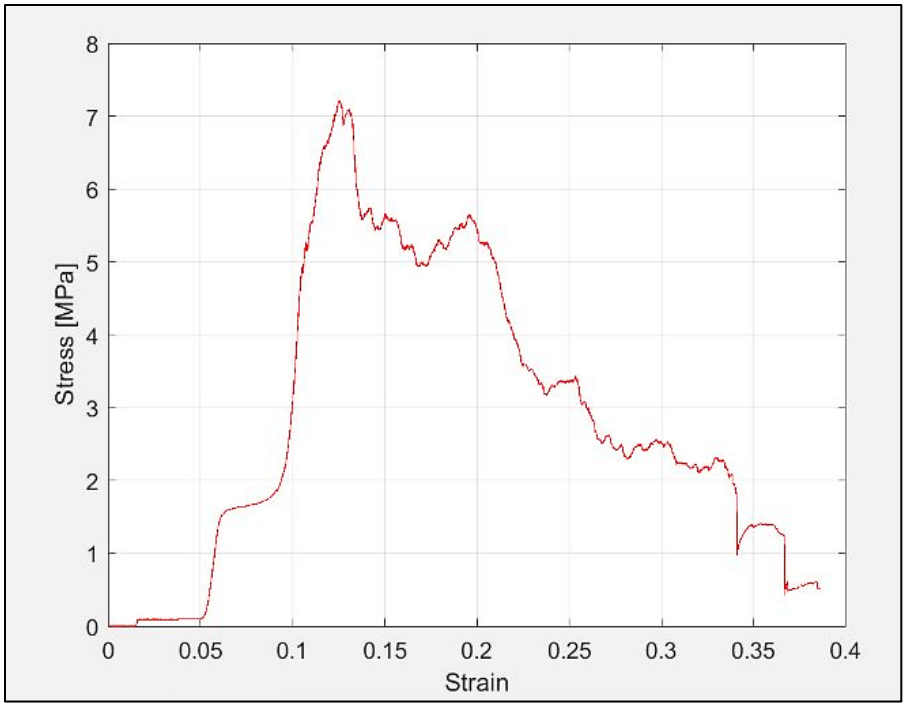

Figure 58. Stress-strain Data for a Molded SiC Cube Under Compression

C. PRINTING TPS MATERIALS

TPS sandwich tiles were designed and modeled using NX 12.0 by Siemens, as shown in Figure 17 (see Chapter II, Section A). These tiles were intended to print via VAP for top and bottom layers and standard thermoplastic extrusion printing for the middle layer. The model was first printed as a prototype with PLA in order to ensure appropriate sizing for testing and analysis, as well as to ensure tolerances were acceptable for each layer. The outer layers were printed with white PLA, while the middle layer was printed with black PLA, as shown in Figure 59.

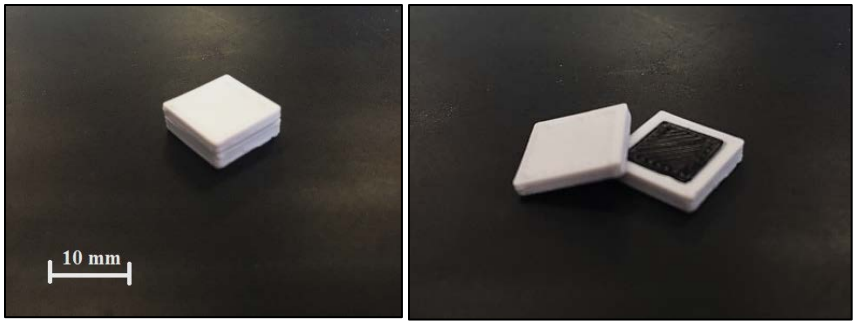

Figure 59. TPS Sandwich Tile Prototype Test Print

Once solid-loaded mixtures were able to produce successful test prints, the mixture was used to print TPS tile components. Several successful parts were printed onto glass slides, one of which is shown in Figure 60. Once printed, the glass slides with the printed parts were fully cured by heating within the vacuum oven, as described in the Curing and Pyrolysis section.

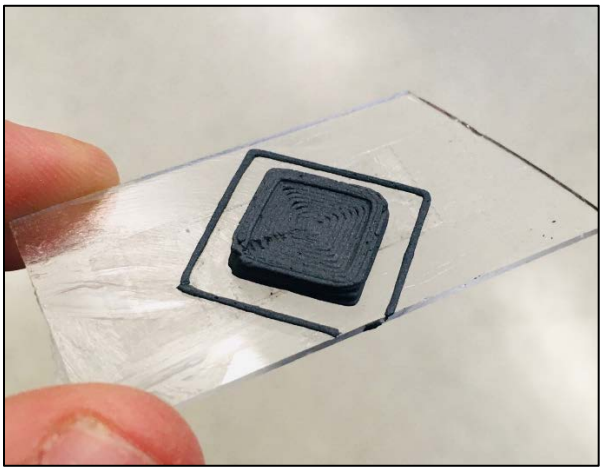

Figure 60. TPS Sandwich Tile Bottom Layer Print with SiC

Once the curing process was complete, the slides were removed from the vacuum oven and cooled. Upon attempting the remove the parts from the slides with a razor blade, the parts broke apart (Figure 61). Since the cured parts could not be safely removed from the slides, another method was introduced for printing and curing SiC parts. Subsequently, the glass slides were tightly wrapped in aluminum foil prior to printing SiC parts with VAP

and coated with a polyvinyl alcohol (PVA)-based glue. This concept was tested with two small hand molds pressed onto glass slides wrapped in aluminum foil, which were then fully cured within the oven (Figure 62). The test samples were then successfully removed from the slide by first removing the foil from the slide, then peeling the foil from the back of the cured part.

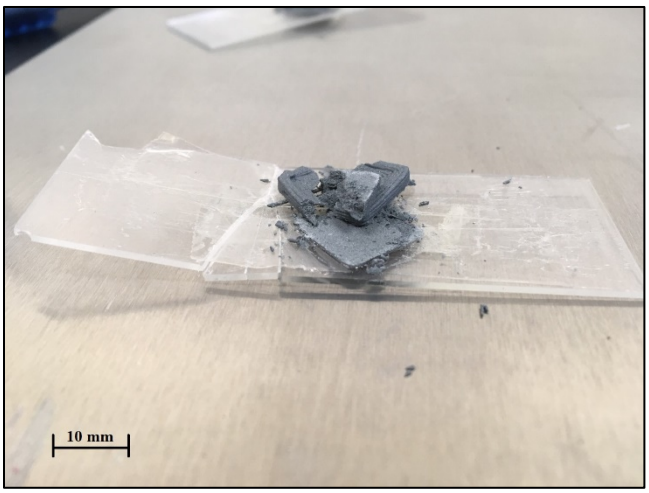

Figure 61. Broken Cured Printed SiC TPS Sandwich Tile Bottom Layer

Figure 62. Aluminum Foil-Wrapped Glass Slides with Test Molds

Finally, several middle layer parts were printed using standard thermoplastic extrusion printing. Six parts each were made from carbon-loaded PLA and carbon-fiber-loaded nylon filaments. Figure 63 (left) depicts a carbon-loaded PLA middle layer placed into VAP printed bottom layer. Bottom and middle layer components were also successfully printed using the dual-extruder printer (see Chapter II, Section C3), as depicted in Figure 63 (right). Due to furnace maintenance delays as well as unforeseen limitations to laboratory access, complete TPS tiles were not assembled and pyrolyzed for additional testing.

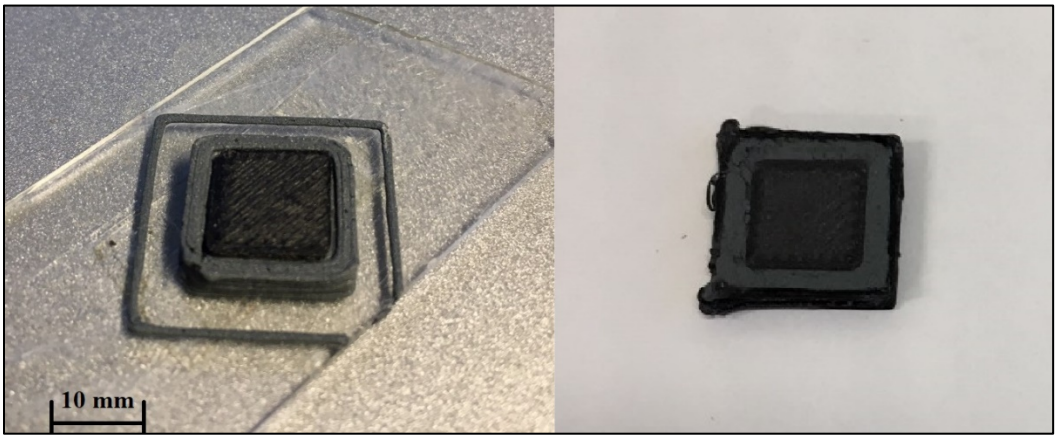

Figure 63. Assembled TPS Tile Bottom and Middle Layers (left) and Dual-extruded TPS Tile Bottom and Middle Layers (right)

Table 9. Summary of Outcomes and Learnings

Section	Outcomes	Learnings
Modeling and simulation	Graphite layer substantially lowered temperatures near the thermal load.	The inclusion of a graphite layer in a sandwich TPS can reduce local temperatures and thermal stress on the TPS (and surface of the spacecraft) which can increase longevity and reliability of the TPS.
Polymer pre-processing and mass loss	10-gram batches of SMP-10 produced more consistent results compared to 1-gram batches. Heating under vacuum also eliminated formation of a cured film on the polymer surface. SMP-10 will thicken with age at room temperature.	Larger batches of SMP-10 will produce more consistent mass loss profiles. Pre-processing fresh SMP-10 at 90°C for 24 hours produced significant (7-9%) mass loss without curing the polymer. SMP-10 will thicken with age (several months) at room temperature and should be refrigerated. If age-thickened, pre-processing at 70°C for 18 hours will also produce a favorable mass loss (~6%) and viscosity for mixing.
Particle size analysis	SiC powder particles ranged from 7–77 µm, with a mean value of 23 µm.	SiC powder particles were sufficiently small for usage in VAP.
Material mixing	Mixture ratio of 80 wt.% SiC powder/20 wt.% SMP-10 produced the best viscosity for VAP. Mixture will heat up from friction during speed mixing, especially at 3,000 RPM. Mixing under vacuum increased mixture density by nearly 10%.	Less solid loading (less SiC powder) produces lower mixture viscosity, leading to increased part creep when printed. More solid loading leads to material breakup in the print nozzle. Heating during mixing can induce curing of the polymer in the mixture; mixing at higher speeds should be kept to short time periods (<10 sec) and followed by active cooling. Air will also become trapped in the mixture while speed mixing, therefore mixing should be done under vacuum.

Section	Outcomes	Learnings
Molding and 3D printing	Molding with various clays led to destroying molded parts when removing them from the molds. Silicone rubber molds proved best for molding SiC parts. Cold bed (0-5°C) printing did not improve print quality. Hot bed (90-150°C) printing marginally, but inconsistently, improved print quality.	Silicone rubber molds are flexible (good for peeling from cured parts) and able to withstand temperatures of first stage curing. Cold and hot bed printing results did not provide improvements that warranted further usage in the study.
Curing and pyrolysis	Initial curing of a molded cube for one hour at 130°C exhibited noticeable expansion compared to a molded cube initially cured for one hour at 100°C. Most parts broke up during pyrolysis under N_2 up to 1,600°C. TGA yielded large mass changes with onsets at ~360°C and 1,300°C.	Initial stage of curing should be conducted ≤100°C at ambient pressure, possibly under an inert gas, to avoid part expansion and oxidation while still allowing gases to escape the material prior to hardening. Pyrolysis must be conducted with a low (2°C/min vice 10°C/min) ramp rate and sufficient (at least one hour) holds at onset temperatures.
SEM	Comparison of images of SiC powder, a cured SiC part, and a pyrolyzed SiC part clearly show the cured SiC part consisted of SiC particles suspended in a cured polymer, while the pyrolyzed part was a crystalline ceramic. Images with pyrolyzed PLA sections show cracking of the ceramic near areas with PLA.	Curing and pyrolysis processes produce ceramic SiC. Interfacing of thermoplastic portions with SiC portions of the TPS must account for differences in thermal expansion and mass loss during pyrolysis.

Section	Outcomes	Learnings
EDS	SiC powder contained Si and C at near-stoichiometric ratios. Cured and pyrolyzed parts contained impurities (mainly oxygen and nitrogen) likely due to the first stage of curing (80°C) in air and pyrolysis under nitrogen.	The first stage of curing should be conducted either under inert gas, or for shorter periods of time compared to the final stage of curing, in order to reduce oxidation of SMP-10. Similarly, pyrolysis should be conducted under argon gas, in order to avoid reaction of SiC with N_2 at high temperatures.
XRD	SiC powder and all pyrolyzed parts exhibited 6H α-phase structure with no broad amorphous peaks.	All the samples showed crystalline structures indicating the pyrolysis target temperature and hold time were sufficient.
Compression testing	One pyrolyzed, molded cube was tested for compressive strength (7.2 MPa), which did not favorably compare with reference data. No additional parts were tested for compressive strength.	It is postulated that the cube that was tested contained cracks and pores from non-optimized curing and pyrolysis procedures that significantly weakened the part. Additional testing of molded parts would need to be conducted to accurately determine compressive strength of CMC-derived SiC parts. Multiple tests with printed SiC parts would need to be conducted to provide an accurate comparison with molded parts.

Section	Outcomes	Learnings
Printing TPS materials	Parts printed directly onto glass slides could not be removed (either before or after curing) without destroying the part due to strong adhesion. Tightly wrapping the glass slide in aluminum foil allowed the part to be removed from the slide prior to pyrolysis. Thermoplastic samples (carbon-loaded PLA and carbon-fiber-loaded nylon) were printed, but not cured and pyrolyzed after being assembled into TPS samples for further analysis. Dual-extrusion of VAP pre-ceramic material with a thermoplastic filament was successful.	Parts should be printed onto something that can later be peeled from it, as the material must be transferred to a vacuum oven for curing without being disturbed, but removed from the surface it was printed on prior to pyrolysis (the glass slide would have melted during pyrolysis in this case). Pyrolysis of middle layer samples was not conducted, so these could not be analyzed to determine which was more suitable for producing a graphite layer in the TPS sandwich. TPS tiles consisting of pre-ceramic material and thermoplastic filament can be printed concurrently, which also improves the ability to remove the printed part from the print bed surface.

IV. CONCLUSIONS

This research explored the feasibility of additively manufacturing a sandwich TPS composite with outer layers of SiC and a carbon-based middle layer. Using computer modeling and simulation, the concept showed great merit. When compared to a similar TPS model composed of only SiC, the model with a carbon middle layer (graphite) showed significant differences local temperatures for at least five minutes of simulated re-entry heating. The graphite layer successfully redistributed heat away from the area subjected to a high thermal load (simulated re-entry), significantly reducing the maximum temperature on the surface of the area subjected to re-entry heating, as well as reducing the maximum temperature of the inner surface of the TPS. This not only provides better protection for a spacecraft in a single flight, but can also improve the longevity of the TPS, thus improving reliability and reducing cost for spacecraft manufacturing and maintenance.

The formulation of a highly viscous mixture capable of producing SiC upon pyrolysis proved feasible with a commercially available SiC powder and pre-ceramic polymer, SMP-10. This was achieved by heating batches of SMP-10 at 90°C for 24 hours under vacuum (70°C for 18 hours for aged, non-refrigerated SMP-10) to induce 6–12% mass loss prior to mixing with -400 mesh SiC powder, at a nominal mixture ratio of 80 wt.% -400 mesh SiC powder and 20 wt.% pre-processed SMP-10. Mixing under vacuum was determined to be crucial as it reduced trapped air in the mixture, thus increasing density of the mixture by nearly 10 wt.%. Full curing of the mixture is best achieved in three stages: (1) four hours at 80°C under normal atmosphere, (2) four hours at 100°C under vacuum, (3) four hours at 250°C under vacuum for a part depth of 6.35 mm. Pyrolysis should include a hold (at least one hour) at 360°C, followed by a shallow ramp rate (2°C/min or less) to 1,300°C with another hold (at least one hour), which will produce a 6H-SiC crystalline ceramic. Continued pyrolysis up to 1,600°C can induce further mass loss as well as produce a cubic crystalline ceramic [22]. One pyrolyzed molded sample included embedded PLA filaments, which remained within the ceramic, indicating that carbon composite structures can be produced using this approach. Pyrolysis should preferably be conducted under an

inert gas, such as argon, or vacuum, as opposed to nitrogen to prevent the formation of Si_3N_4 on the surface of the parts.

Material strength determined from compression testing showed significantly lower values when compared to referenced data for SiC. This was likely attributed to cracks formed in the molded part that was tested, due to early, unrefined procedures in curing and pyrolysis of the part. Additional compression testing on molded and printed parts that have been cured and sintered with refined procedures will need to be conducted to better test and characterize the strength of the material, post-pyrolysis.

Components for all TPS layers were able to be 3D printed using VAP for SiC layers and standard thermoplastic FDM for the middle layer. SiC parts printed with a single extruder exhibited varying degrees of material creep when the height of the part exceeded 3 mm; however, this was generally minimal when printed with a nominally prepared material mixture and relatively large layer heights compared to the nozzle diameter. Additionally, the material creep could be eliminated using a dual-head print method consisting of a VAP extruder and a thermoplastic extruder. Using this dual-extrusion method, the outer shells of each layer are printed with a thermoplastic filament, while the infill is printed with the SiC mixture. The thermoplastic edges serve as a support structure to eliminate material deformation until the SiC mixture is hardened in the first stage of the curing process. These supports can then be safely removed (e.g., using a water-soluble thermoplastic such as PVA) prior to pyrolysis or can be used to form the source of embedded graphite or amorphous carbon in a composite structure.

Middle layer components were 3D printed using two thermoplastics: carbon-loaded PLA and carbon-fiber-loaded nylon. While several components were made using each material, they were not assembled into printed bottom and top SiC layers. Complete TPS tiles, assembled or printed with different middle layer materials, will need to be pyrolyzed to determine which middle layer material produces the best graphitic inner layer. Additional testing should be conducted on the pyrolyzed TPS tiles to evaluate their mechanical strength and thermal properties.

Overall, the concept of a ceramic sandwich TPS composed of SiC and graphite show potential for use in future spacecraft design. Additive manufacturing of the components for this TPS can be accomplished with a combination of VAP and standard FDM. Additional testing with fully assembled models should be able to determine the efficacy of this additively manufactured TPS as well as further refine the processes for its preparation and production.

THIS PAGE INTENTIONALLY LEFT BLANK

V. FUTURE WORK

A. CARBON LAYER OPTIMIZATION

Two different materials were used to 3D print the middle layer of the TPS sandwich; however, since a full TPS sandwich tile was never assembled and pyrolyzed, it was never determined which filament produced an optimal layer for the TPS, or if investigation of other materials was warranted for this application. Completed TPS tiles, some with carbon-loaded PLA and some with carbon-fiber-loaded nylon, should be assembled, cured, and pyrolyzed according to procedures developed in this study. Only then can there be a determination whether the materials produce a suitable carbon layer and if so, which one is a better choice. Additional unknowns may be encountered, resulting in further refinements to the curing and/or pyrolysis processes.

B. ACCURATE DETERMINATION OF MECHANICAL STRENGTH

Mechanical strength of pyrolyzed SiC parts was not adequately determined in this study. Only a single compression test was conducted on a molded cube that was cured and pyrolyzed using unrefined procedures. To more accurately assess the compressive strength of pyrolyzed SiC parts, multiple tests should be conducted on both molded and printed parts that have been prepared using refined curing and pyrolysis procedures. Comparison of data between molded and printed parts would then determine any increase or reduction in strength of printing parts vice molding them. Finally, pyrolyzed TPS tiles should be tested for compressive strength to determine if the addition of a carbon middle layer increases or reduces the strength of parts when compared to the data for pure SiC parts.

C. THERMAL ANALYSIS

Printed and molded SiC parts should be analyzed to determine their material properties, including but not limited to thermal conductivity, specific heat, and coefficient of thermal expansion. Data can be compared to determine whether or not 3D printed porosity produces improved thermal characteristics. Assembled and pyrolyzed TPS tiles should then be tested to determine the efficacy of a carbon middle layer in the redistribution

of heat. If both filament materials produce a suitable carbon layer, analysis from thermal testing may determine which middle layer material will work best for TPS applications.

D. SCALING AND MANUFACTURING OF COMPLEX PARTS

Just as space shuttle orbiter tiles varied in size, shape, and thickness [9], the sandwich TPS segments will likely need to be manufactured in larger sizes with varying shapes (including curved surfaces) and thicknesses. Using the dual-extrusion capability, the 3D printing of larger, more irregular shapes should be conducted to further test the feasibility of additively manufacturing a ceramic sandwich TPS. The varying of the thickness of each layer should also be explored to optimize TPS performance (e.g., a thicker middle layer may more efficiently redistribute heat or a thicker inner SiC layer relative to the outer layer may provide better protection for the surface of the spacecraft). Usage of computer modeling and simulation should provide great insight into these concepts, as well as optimization prior to the manufacture of parts.

E. ALTERNATIVE MATERIALS

This study focused on the use of SiC as a CMC-based TPS, however, alternative CMCs should also be explored for an AM sandwich TPS application. Composites with hafnium (Hf) or zirconium (Zr) can provide protection from higher temperatures than SiC [50]; hafnia and zirconia have higher melting points and resist oxidation above 2,000°C, but multiple solid phase changes at high temperatures results in a corresponding large volume change for each material [51]. Prior work has indicated that silicoboron carbonitride ($Si_{3.0}B_{1.0}C_{4.3}N_{2.0}$) ceramic resists oxidation at high temperatures and is thermally stable up to 2,000°C [52]. Additional research will need to reveal a feasible method for AM of alternative ceramics. Likewise, alternatives to a graphite middle layer should be explored for both improved in-plane thermal conductivity and mechanical strength. High-performance carbon structures such as carbon nanotubes and graphene exhibit such characteristics and have already been incorporated into AM methods [53].

LIST OF REFERENCES

[1] White House, “Space Policy Directive-1,” Washington, DC, USA, 2017. [Online]. Available: https://www.hsdl.org/?view&did=806399

[2] Y. Wang, Z. Chen, and S. Yu, “Ablation behavior and mechanism analysis of C/SiC composites,” *Journal of Materials Research and Technology*, vol. 5, no. 2, pp. 170–182, Apr. 2016, doi: 10.1016/j.jmrt.2015.10.004

[3] S. M. Johnson, “Thermal protection materials and systems: Past, present, and future.” Presentation at Missouri University of Science and Technology, Rolla, MO, USA, April 4, 2013. [Online]. Available: https://ntrs.nasa.gov/search.jsp?R=20130014035 2019–04-14T02:09:39+00:00Z

[4] Federal Aviation Administration, “Returning from space: Re-entry.” Online tutorial. Accessed January 9, 2020. [Online]. Available: https://www.faa.gov/about/office_org/headquarters_offices/avs/offices/aam/cami/library/online_libraries/aerospace_medicine/tutorial/media/iii.4.1.7_returning_from_space.pdf

[5] G. Chapline, A. Rodriguez, C. Snapp, G. Dorsey, M. Fowler, B. Greene, W. Schneider, C. Scott, M. Pessin, J. Butler, J. S. Sparks, P. Bauer, B. Steinetz, C. Stevenson, “Thermal protection systems,” NASA. Accessed October 14, 2019. [Online]. Available: Ahttps://www.nasa.gov/centers/johnson/pdf/584728main_Wings-ch4b-pgs182-199.pdf

[6] Columbia Accident Investigation Board, “Chapter 3: Accident Analysis,” Washington, DC, USA, August 2003. [Online]. Available: http://s3.amazonaws.com/akamai.netstorage/anon.nasa-global/CAIB/CAIB_lowres_chapter3.pdf

[7] J. E. Puulosky, S. Leger, “Apollo experience report—Thermal protection subsystem ,” NASA, Washington, DC, USA, Rep D-7564, 1974. [Online]. Available: https://ntrs.nasa.gov/search.jsp?R=19740007423

[8] B. K. Bessire, S. A. Lahankar, and T. K. Minton, “Pyrolysis of phenolic impregnated carbon ablator (PICA),” *ACS Appl. Mater. Interfaces*, vol. 7, no. 3, pp. 1383–1395, Jan. 2015, doi: 10.1021/am507816f

[9] National Aeronautics and Space Administration, “Space shuttle tiles.” Accessed December 21, 2019. [Online]. Available: https://www.nasa.gov/sites/default/files/atoms/files/shuttle_tiles_9_12v2.pdf

[10] National Aeronautics and Space Administration, “Supplemental space shuttle tile lesson.” Accessed December 21, 2019. [Online]. Available: https://www.nasa.gov/sites/default/files/atoms/files/space_shuttle_tiles_9_12_supplemental.pdf

[11] M. L. Blosser, C. J. Martin, K. Daryabeigi, and C. C. Poteet, “Reusable metallic thermal protection systems development,” NASA Langley Research Center, Hampton, VA, USA. Accessed April 7, 2019. [Online]. Available: https://ntrs.nasa.gov/search.jsp?R=20040095922

[12] M. Lacoste, F. Fenot, A. Lacombe, and M. Cataldi, “Using C/SiC composite materials for thermal protection system for planetary entry system, behaviour in relevant environment,” presented at the International Conference on Environmental Systems, 1995, p. 951617, doi: 10.4271/951617

[13] W. Krenkel, “Carbon fiber reinforced CMC for high-performance structures,” *International Journal of Applied Ceramic Technology*, vol. 1, no. 2, pp. 188–200, Jan. 2005, doi: 10.1111/j.1744-7402.2004.tb00169.x

[14] B. Esser *et al.*, “Innovative thermal management concepts and material solutions for future space vehicles,” *Journal of Spacecraft and Rockets*, vol. 53, no. 6, pp. 1051–1060, Nov. 2016, doi: 10.2514/1.A33501

[15] K. Keller, E. Pfeiffer, P. Gaudenzi, L. Lampani, T. Ullmann, and H. Ritter, “Smart thermal protection systems,” presented at the International Conference On Environmental Systems, 2005, pp. 2005–01–2901, doi: 10.4271/2005-01-2901

[16] M. C. Sulkis, J. Driver, A. Saade-Castillo, A. Thompson, H. Wu, and J. H. Koo, “Additive manufacturing of thermal protection system materials,” in *2018 AIAA/ASCE/AHS/ASC Structures, Structural Dynamics, and Materials Conference*, Kissimmee, Florida, 2018, doi: 10.2514/6.2018-0092

[17] S. A. M. Tofail, E. P. Koumoulos, A. Bandyopadhyay, S. Bose, L. O’Donoghue, and C. Charitidis, “Additive manufacturing: Scientific and technological challenges, market uptake and opportunities,” *Materials Today*, vol. 21, no. 1, pp. 22–37, Jan. 2018, doi: 10.1016/j.mattod.2017.07.001

[18] T. Wohlers and T. Gornet, “History of additive manufacturing,” *Wohlers Report 2014*. Fort Collins, CO, USA, August 2014.

[19] D.L. Bourell, J.J. Beaman, H.L. Marcus, and J.W. Barlow, “Solid freeform fabrication: An advanced manufacturing approach,” *Proc. Solid Freeform Fabricaton Symposium* 1–7 (1990).

[20] I. E. Gunduz, M. S. McClain, P. Cattani, G. T.-C. Chiu, J. F. Rhoads, and S. F. Son, “3D printing of extremely viscous materials using ultrasonic vibrations,” *Additive Manufacturing*, vol. 22, pp. 98–103, Aug. 2018, doi: 10.1016/j.addma.2018.04.029

[21] M.S. McClain, I.E. Gunduz, S.F. Son, “Additive manufacturing of ammonium perchlorate composite propellant with high solids loadings,” *Proceedings of the Combustion Institute*, vol. 37, no. 3, pp. 3135–3142, 2019, [Online]. doi: https://doi.org/10.1016/j.proci.2018.05.052

[22] S. A. Potticary, “Chemical and behavioral study of commercial polycarbosilanes for the processing of SiC fibers,” M.S. thesis, Dept. of Mech. and Mat. Eng., Univ. of Cincinnati, Cincinnati, OH, USA, 2017.

[23] P. Colombo, G. Mera, R. Riedel, and G. D. Sorarù, “Polymer-derived ceramics: 40 years of research and innovation in advanced ceramics,” *Journal of the American Ceramic Society*, Jun. 2010, doi: 10.1111/j.1551-2916.2010.03876.x

[24] D. King, Z. Apostolov, T. Key, C. Carney, and M. Cinibulk, “Novel processing approach to polymer-derived ceramic matrix composites,” *Int J Appl Ceram Technol*, vol. 15, no. 2, pp. 399–408, Mar. 2018, doi: 10.1111/ijac.12805

[25] X. Qian, Q. Zhou, and L. Ni, “Preceramic polymer as precursor for near-stoichiometric silicon carbon with high ceramic yield,” *J. Appl. Polym. Sci.*, vol. 132, no. 4, p. n/a-n/a, Jan. 2015, doi: 10.1002/app.41335

[26] P. Greil, “Polymer derived engineering ceramics,” *Advanced Engineering Materials*, vol. 2, no. 6, pp. 339–348, Jun. 2000. [Online]. doi: 10.1002/1527-2648

[27] Diptanshu, Guanxiong Miao, Chao Ma, “Vat photopolymerization 3D printing of ceramics: Effects of fine powder,” *Manufacturing Letters*, vol. 21, pp. 20–23, Aug. 2019. [Online]. doi: https://doi.org/10.1016/j.mfglet.2019.07.001

[28] M. S. McClain, I. E. Gunduz, and S. F. Son, “Additive Manufacturing of Carbon Fiber Reinforced Silicon Carbide Solid Rocket Nozzles,” in AIAA Scitech 2019 Forum, San Diego, California, Jan. 2019, doi: 10.2514/6.2019-0408.

[29] Siklitsky, V, “SiC – Silicon carbide,” Forum SiC on Physical Properties of Semiconductors, NSM-archive. Accessed January 13, 2020. [Online]. Available: http://www.ioffe.ru/SVA/NSM/Semicond/SiC/basic.html

[30] AZO Materials, “Silicon Carbide (SiC) Properties and Applications.” Accessed January 13, 2020. [Online]. Available: https://www.azom.com/properties.aspx?ArticleID=42

[31] AZO Materials, “Graphite (C) – Classifications, Properties & Applications.” Accessed: January 13, 2020. [Online]. Available: https://www.azom.com/article.aspx?ArticleID=1630

[32] University of Texas at Austin Microelectronics Research Center, “SEM ZEISS Neon 40 - Bruker EDS - Raith Elphy pattern generator,” 2013. [Online]. Available: https://www.mrc.utexas.edu/facilities/equipment/sem-zeiss-neon-40-bruker-eds-raith-elphy-pattern-generator

[33] Nanoscience Instruments, “Scanning electron microscopy,” 2020. [Online]. Available: https://www.nanoscience.com/techniques/scanning-electron-microscopy/

[34] Jove, “Scanning electron microscopy (SEM).” [Online]. Available: https://www.jove.com/science-education/5656/scanning-electron-microscopy-sem

[35] S. Ebnesajjad, *Surface Treatment of Materials for Adhesive Bonding, Second Edition*. Oxford: William Andrew, 2014.

[36] Horiba, *LA-950 Laser Particle Size Analyzer*. [Online]. Available: https://www.horiba.com/scientific/products/particle-characterization/zeta-potential-analysis/details/la-950-laser-particle-size-analyzer-108/

[37] Netzsch, *Simultaneous Thermal Analyzer – STA 449 F3 Jupiter*. [Online]. Available: https://d2brmtk65c6tyc.cloudfront.net/media/thermal-analysis/brochures/STA_449_F3_Jupiter_en_web.pdf

[38] PerkinElmer, *Thermogravimetric Analysis: A Beginner’s Guide*, 009380C_01, 2015. [Online]. Available: https://www.perkinelmer.com/lab-solutions/resources/docs/FAQ_Beginners-Guide-to-Thermogravimetric-Analysis_009380C_01.pdf

[39] W. Groenewoud, *Characterization of Polymers by Thermal Analysis*, Hertogenbosch, The Netherlands: Elsevier Science, 2001.

[40] Hitachi, “Principle of differential scanning calorimetry (DSC),” 2020. [Online]. Available: https://www.hitachi-hightech.com/global/products/science/tech/ana/thermal/descriptions/dsc.html

[41] Rigaku, “Rigaku introduces new 5th generation miniflex benchtop x-ray diffraction (XRD) instrument,” January 15, 2012. [Online]. Available: https://www.rigaku.com/press/sun-01152012-1200/746050664

[42] A. K. Chatterjee, “X-ray diffraction,” in *Handbook of Analytical Techniques in Concrete Science and Technology*, V. S. Ramachandran and J. J. Beaudoin, Eds. Ottawa, Ontario, Canada: William Andrew Publishing/Noyes Publications, 2001, pp. 275–332.

[43] X. Wan, “Carbothermal synthesis of silicon nitride,” Ph.D. dissertation, School of M.S. and Eng., Univ. of New S. Wales, Kensington, Australia, 2013. [Online]. Available: http://unsworks.unsw.edu.au/fapi/datastream/unsworks:11666/SOURCE01?view=true

[44] G. C. Capitani, S. Di Pierro, and G. Tempesta, “The 6H-SiC structure model: Further refinement from SCXRD data from a terrestrial moissanite,” American Mineralogist, vol. 92, no. 2–3, pp. 403–407, Feb. 2007, doi: 10.2138/am.2007.2346

[45] R. He, G. Ding, K. Zhang, Y. Li, and D. Fang, “Fabrication of SiC ceramic architectures using stereolithography combined with precursor infiltration and pyrolysis,” *Ceramics Int’l*, vol. 45, no. 11, pp. 14006-14014, 2019. [Online]. doi: https://doi.org/10.1016/j.ceramint.2019.04.100

[46] P. Neudeck, “Silicon carbide technology,” *The VLSI Handbook, Second Ed*., vol. 20061800, pp. 5–1 – 5–34, Dec. 2006. [Online]. Available: https://ntrs.nasa.gov/archive/nasa/casi.ntrs.nasa.gov/20150022213.pdf

[47] L. Wang, S. Dimitrijev, J. Han, F. Iacopi, and J. Zou, “Transition between amorphous and crystalline phases of SiC deposited on Si substrate using H3SiCH3,” *Journal of Crystal Growth*, vol. 311, no. 19, pp. 4442–4446, Sep. 2009, doi: 10.1016/j.jcrysgro.2009.07.036

[48] Pam-Xiamen, *Property of Silicon Carbide (SiC)*, 2013. [Online]. Available: http://www.qualitymaterial.net/news_list85.html

[49] Accuratus, *Silicon Carbide, SiC Ceramic Properties*, 2013. [Online]. Available: https://www.accuratus.com/silicar.html

[50] D. E. Glass, “Ceramic matrix composite (CMC) thermal protection systems (TPS) and hot structures for hypersonic vehicles,” presented at 15th AIAA Int’l Space Planes and Hypersonic Sys and Tech Conf, Dayton, OH, USA, Apr 28 – May 1, 2008. [Online]. doi: https://doi.org/10.2514/6.2008-2682

[51] K. Upadhya, J. M. Yang, W. Hoffman, “Advanced materials for ultrahigh temperature applications above 2000°C,” *Amer. Ceram. Soc. Bull. 76:23*, Nov. 1997. [Online]. Available: https://www.researchgate.net/publication/235012461_Advanced_Materials_for_Ultrahigh_Temperature_Structural_Applications_Above_2000_deg_C

[52] R. Riedel, A. Kienzle, W. Dressler, L. Ruwisch, J. Bill, and F. Aldinger, “A silicoboron carbonitride ceramic stable to 2,000°C,” *Nature*, vol. 382, no. 6594, pp. 796–798, Aug. 1996, doi: 10.1038/382796a0

[53] S. F. A. Acquah *et al.*, “Carbon nanotubes and graphene as additives in 3D printing,” in *Carbon Nanotubes - Current Progress of their Polymer Composites*, M. R. Berber and I. H. Hafez, Eds. InTech, 2016.

INITIAL DISTRIBUTION LIST

1. Defense Technical Information Center
   Ft. Belvoir, Virginia

2. Dudley Knox Library
   Naval Postgraduate School
   Monterey, California